Spin-S impurities with XXZ anisotropy in a spin-$\frac{1}{2}$ Heisenberg chain

Ayushi Singhania [ORCID],[1,*] Masahiro Kadosawa,[2] Yukinori Ohta [ORCID],[2] Sanjeev Kumar [ORCID],[1] and Satoshi Nishimoto [ORCID][3,4]

[1]*Department of Physical Sciences, Indian Institute of Science Education and Research Mohali,*
Sector 81, S.A.S. Nagar, Manauli PO 140306, India
[2]*Department of Physics, Chiba University, Chiba 263-8522, Japan*
[3]*Department of Physics, Technical University Dresden, 01069 Dresden, Germany*
[4]*Institute for Theoretical Solid State Physics, IFW Dresden, 01069 Dresden, Germany*

We study the effect of anisotropy of spin-S impurities on an antiferromagnetic SU(2) Heisenberg chain. The magnetic impurities are assumed to have an XXZ-type anisotropic exchange with their neighboring sites. First, using density-matrix renormalization group technique, we examine spin-spin correlation function, instability of Néel order, and local spin susceptibility in the presence of a single spin-S impurity. Based on the results, we find that the types of spin-S impurities are classified into two groups: (i) nonmagnetic and $S = 1$ impurities enhance only short-range antiferromagnetic correlation and (ii) $S = \frac{1}{2}$ and $S > 1$ impurities can, in contrast, stabilize a long-range Néel order in the disordered SU(2) Heisenberg chain. Then, we focus on the case of $S = \frac{1}{2}$ impurity as a representative of (ii) and investigate the evolution of some experimentally observable quantities such as magnetization, specific heat, and magnetic susceptibility, as a function of concentration and XXZ anisotropy strength of the impurity. We confirm that the Néel order is induced in the bulk spin chain in the presence of finite amount of easy-axis XXZ $S = \frac{1}{2}$ impurities. Furthermore, we recover some of the aforementioned features using cluster mean-field theory, which allows us to present results on experimentally accessible quantities at finite temperatures. Interestingly, in the presence of uniform magnetic field, the total magnetization exhibits a pseudogap behavior for low values of applied field. We also discuss the dependence of NMR spectrum on various XXZ impurities and identify that the spin state of Co impurity in $SrCu_{0.99}Co_{0.01}O_2$ is $S = \frac{3}{2}$.

I. INTRODUCTION

It is well known that the presence of impurities in solids can lead to quantitative changes in their properties. For example, a disordered metal is expected to have higher resistivity compared to a defect-free metal [1], transition temperature to superconducting order can be altered by the presence of impurities [2], etc. However, in some cases, the presence of impurities can even modify the qualitative behavior of the system. For instance, metals can turn into insulators due to disorder-induced phenomenon known as Anderson localization [3,4]. Such a qualitative change of behavior can also occur in magnets. A famous example is the disorder-induced change in the order of phase transitions [5]. Defects in magnetic materials can modify not only the ground-state properties, but also the excitation spectrum [6]. Substitution of a magnetic ion by a different ion with the same or different spin, or a magnetic ion coupled to random spin in a lattice, corresponds to the presence of defects [7]. Low-dimensional systems are very sensitive to disorder and often display dramatic effects in the presence of impurities due to interplay between quantum effects, strong correlations, and disorder [8].

Some observations of impurity-induced effects in spin systems are emergence of $S = \frac{1}{2}$ degrees of freedom at the edges,

which occurs when Cu is doped in a Haldane material [9]. A low concentration of nonmagnetic impurities induces a long-range magnetic order in spin-Peierls material $CuGeO_3$ [10,11]. Similar observations have been made for a two-leg spin-$\frac{1}{2}$ ladder compound $SrCu_2O_3$, where doping of as low as 1% Zn ($S_{imp} = 0$) results in antiferromagnetic (AFM) behavior; we denote the magnitude of impurity spin by S_{imp} and a nonmagnetic impurity is expressed as $S_{imp} = 0$. Furthermore, it was shown that corresponding Néel temperature can be increased with increase in concentration of impurities [12]. Several experimental studies have been performed on spin-$\frac{1}{2}$ materials Sr_2CuO_3 and $SrCuO_2$, which are considered good realizations of one-dimensional (1D) Heisenberg model [13].

Experimental investigations, on the other hand, reveal an enhancement of long-range order on the introduction of Zn^{2+} ($S_{imp} = 0$) in $SrCuO_2$ (zigzag chain) and Sr_2CuO_3 (linear chain) [14]. Whereas, substitution of $S_{imp} = 1$ impurity in a spin-$\frac{1}{2}$ Heisenberg chain is known to result in a Kondo singlet where the impurity spin is Kondo screened by the two neighboring spins of the chain. Similar to nonmagnetic substitution, formation of singlets at $S_{imp} = 1$ impurity site disrupts the translational invariance of the chain, breaking it into finite lengths. This leads to confinement of spinons and results in emergence of a spin gap in low-lying excitations. This has been confirmed experimentally for low concentration of Ni ($S_{imp} = 1$) doping in $SrCuO_2$, where sizable spin pseudogap appears as a consequence of impurities [15]. While experimental results reveal that doping of $S_{imp} = 0, 1$

*Present address: Institute for Theoretical Solid State Physics, IFW Dresden, 01069 Dresden, Germany.

in spin chain materials suppresses long-range magnetic ordering temperature [16]. Investigations of replacing a spin-$\frac{1}{2}$ magnetic ion (Cu^{2+}) with another spin-$\frac{1}{2}$ ion (Co^{2+}) in spin chain material $SrCuO_2$ reveal that the bulk behavior switches from Heisenberg to Ising type. Due to this, Ising-type (or XXZ-type) anisotropy-induced magnetic ordering temperature is enhanced; however, the gapless nature of the spin excitations is not disturbed. Similar behaviors of Néel-type ordering appear in Co-based spin-$\frac{1}{2}$ Ising chain compounds $BaCo_2V_2O_8$ [17] and $SrCo_2V_2O_8$ [18]. However, in the Co-doped $SrCuO_2$, the spin-lattice relaxation rates T_1^{-1} do not obey the gaplike decrease, and the possibility of Co^{2+} acting as a spin-$\frac{3}{2}$ ion has also been suggested [19].

Theoretical efforts using field theory, renormalization arguments [7,20], and numerical methods like quantum Monte Carlo [21,22] have been successfully employed to investigate properties of low-dimensional materials when doped with magnetic (specifically $S_{imp} = 1$) and nonmagnetic impurities. Field-theoretical and numerical studies using density-matrix renormalization group (DMRG) of isotropic spin-$\frac{1}{2}$ impurity coupled to spin-$\frac{1}{2}$ chain expects the impurity spin to be over-screened in analogy to Kondo effect [20,23,24]. However, experimental results with $S_{imp} = \frac{1}{2}$ embedded in the chain stress the importance of anisotropic effects. Also, very few studies have been carried out on the effect of magnetic impurity with $S_{imp} > 1$.

In this paper, motivated by the above situation, we consider the spin-$\frac{1}{2}$ AFM Heisenberg chain doped with XXZ-type anisotropic spin-S impurities using DMRG technique and cluster mean-field theory (CMFT) approach. Based on the ground-state properties in the presence of a single spin-S impurity, we find that the types of spin-S impurities are classified into two groups: (i) nonmagnetic and $S = 1$ impurities enhance only short-range antiferromagnetic correlation and (ii) $S = \frac{1}{2}$ and $S > 1$ impurities can, in contrast, stabilize a long-range Néel order in the disordered SU(2) Heisenberg chain. Then, we focus on the case of $S = \frac{1}{2}$ impurity as a representative of (ii) in the latter part of this paper. We thus confirm that the Néel order is induced in the bulk spin chain in the presence of finite amount of easy-axis XXZ $S = \frac{1}{2}$ impurities and the corresponding staggered magnetization increases with increasing the impurity density as well as the anisotropy strength. Interestingly, in presence of uniform magnetic field, total magnetization exhibits a pseudogap behavior for low values of applied field. We also show that some of the above features can be obtained using CMFT. This allows us to discuss the finite-temperature behavior of the model in the context of real materials, where the spin chains are typically weakly coupled to each other and finite-temperature phase transitions are possible.

The remainder of the paper is organized as follows: In Sec. II, we explain the spin-$\frac{1}{2}$ AFM Heisenberg model doped with XXZ-type anisotropic spin-S impurities and describe the numerical methods applied. In Sec. III, we examine the effect of spin-S XXZ impurities on the ground-state properties. In Sec. IV, the temperature dependence of specific heat and spin susceptibility as functions of the impurity density and the anisotropy strength is discussed. Section V provides a summary and conclusions.
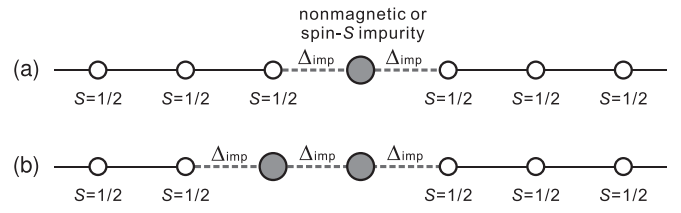

FIG. 1. (a) A schematic view of spin-$\frac{1}{2}$ Heisenberg chain with an internal nonmagnetic (vacancy) or spin-S impurity (filled circle). The exchange interaction on the undoped chain is spin isotropic (solid line) and that between the magnetic impurity and its neighboring sites can be of the XXZ type. In (b), two impurities sit on adjacent sites.

II. MODEL AND METHOD

A. Impurity-doped spin-$\frac{1}{2}$ Heisenberg chain

We consider a spin-$\frac{1}{2}$ AFM Heisenberg chain and replace a finite number of sites with spin-S impurities. The impurities are assumed to have an XXZ-type easy-axis anisotropy on the interaction links with their neighbors. The Hamiltonian reads as

$$\mathcal{H} = \sum_{i \notin imp} \left[\frac{1}{2}(S_i^+ S_{i+1}^- + S_i^- S_{i+1}^+) + S_i^z S_{i+1}^z \right]$$
$$+ \sum_{j \in imp} \left[\frac{1}{2}(S_{j-1}^- + S_{j+1}^-)S_{imp,j}^+ + \text{H.c.} \right.$$
$$\left. + \Delta_{imp}(S_{j-1}^z + S_{j+1}^z)S_{imp,j}^z \right], \qquad (1)$$

where $\mathbf{S}_i$ is spin-$\frac{1}{2}$ operator at nonimpurity site i, $\mathbf{S}_{imp,j}$ is spin-S operator at impurity site j, and Δ_{imp} is the XXZ anisotropy of the interaction between the impurity and neighboring sites. We assume that the undoped chain is spin isotropic [see Fig. 1(a)]. The interaction between adjacent impurities is also XXZ anisotropic with Δ_{imp} [see Fig. 1(b)]. The impurity density n_{imp} is defined as the ratio of N_{imp}/N_c, where N_{imp} is number of impurities embedded in the chain consisting of N_c spins. Note that, in the limit of $n_{imp} = 1$ for $S_{imp} = \frac{1}{2}$, the Hamiltonian is reduced to a spin-$\frac{1}{2}$ Heisenberg chain with the uniform XXZ anisotropy Δ_{imp}.

For a given set of N_{imp} and N_c, the positions of impurities are randomly distributed. Then, setting the length of nonimpurity chain between two impurities to be l, the distribution function of existing probability is given by

$$P(l) = n_{imp} \exp\left[-\frac{n_{imp}}{\sqrt{1 - n_{imp}}} l \right]. \qquad (2)$$

The mean length of nonimpurity chain is $\bar{l} = (1 - n_{imp})/n_{imp}$.

B. Density-matrix renormalization group

To examine the ground-state properties of impurity-doped chain, we employ the DMRG technique, which is a powerful numerical method for various 1D quantum systems [25]. Although the DMRG is basically restricted to the ground-state calculations, very long chains with order of a few thousand

sites can be studied with high accuracy. Hence, a good realization of randomly distributed impurities close to the bulk limit is possible. We keep up to $m = 6000$ density-matrix eigenstates in the renormalization procedure. In this way, the discarded weight is less than 1×10^{-13}. However, the DMRG wave function frequently tends to get trapped in a "false" (or metastable) ground state when we study disordered systems. Thus, we need to pay special attention to the convergence of calculation, for example, by such actions as confirming the unchanged convergence even with different initial conditions. Either open or periodic boundary condition is chosen, depending on the calculated quantities.

C. Cluster mean-field technique

We also utilize CMFT to study the Hamiltonian with spin-$\frac{1}{2}$ XXZ impurities on 1D isotropic SU(2) cluster. The CMFT is an extension of a single-site Weiss mean-field (MF) theory, where instead of a single site we consider a cluster comprising of N_c spins. For 1D system, the edge spins $\mathbf{S}_1$ and $\mathbf{S}_{N_c}$ couple to neighboring cluster via standard mean-field decoupling. Since there are numerous ways in which impurity sites can be distributed, we average observables over various random configurations N_{av} for a fixed number of impure sites. The edge spins are forced to remain pure in a random configuration to avoid explicit dependence of anisotropy due to the MF decoupling. As a result, the impurity density n_{imp} can reach a maximum of $(N_c - 2)/N_c$. We present results computed for a cluster of 10 spins (unless specified otherwise). Calculations are also performed for larger cluster sizes for scaling analysis.

The CMFT enables us to study phase transition in thermodynamic properties within a given cluster size. Although the Mermin-Wagner theorem rigorously forbids finite-temperature phase transition associated with a spontaneous symmetry breaking in pure 1D systems due to thermal and quantum fluctuations, we may argue that any symmetry-breaking MF-type treatment of quantum systems should provide a finite-temperature phase transition. However, this becomes physically relevant for real systems where the 1D spin chains are typically weakly coupled with neighboring chains and finite transition temperatures are experimentally observed. The transition temperatures may well be low if partial inclusion of quantum fluctuations is achieved by, e.g., the CMFT as in the present case. Most importantly, the dependence of transition temperatures on the strength of anisotropy and concentration of impurities as obtained via CMFT can provide direct experimentally measurable consequences of such impurity doping.

III. GROUND-STATE PROPERTIES

A. Influence of single impurity on spin-spin correlations

We begin by investigating the effects of single XXZ spin-S impurity on a spin-$\frac{1}{2}$ Heisenberg chain, a good representation of very low concentration of magnetic impurities in a real material. To do so, we first calculate the distance dependence of spin-spin correlation functions from the impurity. Since an AFM Heisenberg chain is considered, we need to focus mainly on the staggered spin-spin correlation function, which
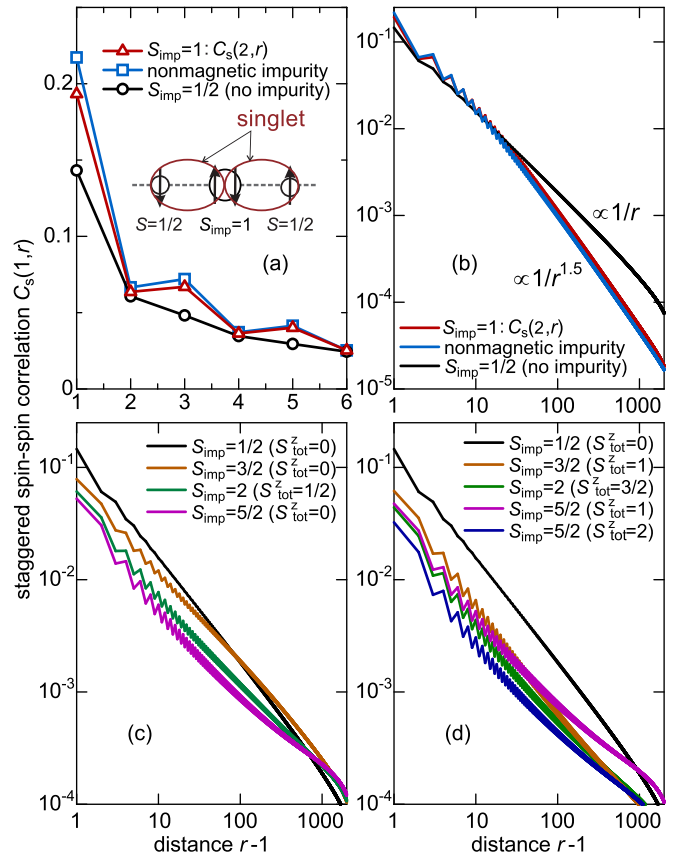

FIG. 2. (a), (b) DMRG results for the staggered spin-spin correlation $C_s(1, r)$ with nonmagnetic impurity and $C_s(2, r)$ with $S_{imp} = 1$ impurity. Inset in (a): structure of two spin-singlet pairs around the $S_{imp} = 1$ impurity. (c), (d) Log-log plots of $C_s(1, r)$ with $S_{imp} > 1$ impurities. In each plot the spin-spin correlation of the bulk SU(2) Heisenberg chain is shown as a reference.

is defined as

$$C_s(i, j) = (-1)^{|i-j|} \langle S_i^z S_j^z \rangle, \tag{3}$$

where $\langle \mathcal{O} \rangle$ denotes expectation value of operator $\mathcal{O}$ in the ground state. A site next to impurity is indexed by "1."

1. Nonmagnetic impurity

In the case of nonmagnetic impurity ($S_{imp} = 0$), i.e, vacancy, an enhancement of short-range staggered spin-spin correlations near the impurity has been theoretically suggested [26,27]. We here confirm it and also see the long-range spin-spin correlation from the impurity. Since the original spin chain is simply cut by a nonmagnetic impurity, no correlations exist between spins on both sides of the nonmagnetic impurity. Therefore, we only need to study an open chain. In Fig. 2(a), the short-range behavior of staggered spin-spin correlation function $C_s(1, r)$ for $S_{imp} = 0$ is compared to that of a bulk SU(2) Heisenberg chain without impurity. We see that the AFM correlation between site at 1 and 2 is significantly increased from $C_s(1, 2) = 0.1456$ for the bulk chain to $C_s(1, 2) = 0.2172$ for $S_{imp} = 0$ impurity. These values agree perfectly to those from the Bethe-ansatz analysis [28]. Furthermore, such an enhancement of $C_s(1, r)$ is seen at certain

distances ($r \lesssim 10$) especially for even r. This is consistent with the previous numerical study [27]. Then, we explore what happens in the correlation at large distances. Figure 2(b) shows log-log plots of $C_s(1, r)$ as a function of distance from the $S_{imp} = 0$ impurity. It is confirmed that the staggered oscillations are maintained indefinitely because $C_s(1, r)$ exhibits an asymptotic behavior with keeping its positive value. The decay rate is $\propto r^{-1.5}$. On the other hand, as is well known, the spin-spin correlation of the bulk SU(2) Heisenberg chain decays as $\propto r^{-1}$ [see Fig. 2(b)]. The decay of $C_s(1, r)$ for nonmagnetic impurity is obviously faster than that for the bulk chain. In short, the short-range staggered spin-spin correlation is indeed enhanced by nonmagnetic impurity but the long-range correlation is rather suppressed.

2. Magnetic impurity with $\Delta_{imp} = 1$

We then examine the effect of magnetic impurity. Unlike the case of nonmagnetic impurity, the spins on both sides of magnetic impurity are still correlated. Hence, only the replacement of open-chain ends by magnetic impurities is not adequate to evaluate the effect of the magnetic impurity. Therefore, we shall proceed as follows: We prepare an open long SU(2) Heisenberg chain with length 2000–4000 and replace the 500th site from one end by a magnetic impurity; and then, calculate the correlation $C_s(1, r + 1)$ with setting the 501th site as $i = 1$, where the distance r is counted towards another chain end. In this way, the Friedel oscillations arising from the open ends can be negligibly small around the impurity at 500th site. We have also confirmed that the results are unchanged even if the position of magnetic impurity is shifted by a few sites from 500th site. First, we restrict ourselves to the case of $\Delta_{imp} = 1$.

Interestingly, the results for $S_{imp} = 1$ impurity are even quantitatively similar to those for nonmagnetic impurity. As seen in Fig. 2(a), the staggered spin-spin correlation is significantly enhanced around the $S_{imp} = 1$ impurity, e.g., $C_s(2, 3) = 0.1933$ in contrast to $C_s(1, 2) = 0.1456$ for the bulk chain. Note that we look at $C_s(2, j)$ instead of $C_s(1, j)$ in the $S_{imp} = 1$ case. This can be explained as follows: The $S_{imp} = 1$ impurity is fractionalized into two spin $\frac{1}{2}$'s and each of them forms a spin singlet with the neighboring spin-$\frac{1}{2}$ site. Accordingly, the $S_{imp} = 1$ impurity and the neighboring two spin $\frac{1}{2}$'s are screened, and the three sites may behave like a nonmagnetic impurity [see the inset of Fig. 2(a)]. Therefore, in the physical sense it is more reasonable to see not $C_s(1, j)$ but $C_s(2, j)$ in the $S_{imp} = 1$ case. Thus, we find that the values of $C_s(2, j)$ for $S_{imp} = 1$ impurity are almost equivalent to those of $C_s(1, j)$ for nonmagnetic impurity at short distance. Furthermore, it is surprising that the asymptotic behavior of $C_s(2, j)$ for $S_{imp} = 1$ impurity is $\propto r^{-1.5}$ as that of $C_s(1, j)$ for nonmagnetic impurity [see Fig. 2(b)]. It seems that the influence of nonmagnetic and $S_{imp} = 1$ impurities on the spin-spin correlations is almost identical even in the quantitative sense, although it would be a natural consequence of the fact that an $S_{imp} = 1$ impurity behaves like a nonmagnetic impurity. This also implies that the valence bond formations of the $S_{imp} = 1$ impurity and its neighboring sites are quite robust.

Moreover, the staggered spin-spin correlation in the presence of higher-S magnetic impurities ($S_{imp} > 1$) is inves-

tigated. In Figs. 2(c) and 2(d), we plot DMRG results for $C_s(1, j)$ with $S_{imp} > 1$ impurities, where the correlation of the bulk SU(2) Heisenberg chain is also shown as a reference data. Note that when the SU(2) Heisenberg chain is doped with a spin-isotropic ($\Delta_{imp} = 1$) $S_{imp} > 1$ impurity, the ground state is degenerate in the $S_{tot}^z = 0, 1, \ldots, S_{imp} - \frac{1}{2}$ sectors for odd S_{imp} and in the $S_{tot}^z = \frac{1}{2}, \frac{3}{2}, \ldots, S_{imp} - \frac{1}{2}$ sectors for even S_{imp}. Accordingly, the results for the ground state in the lowest S_{tot}^z sector for each S_{imp} impurity are plotted in Fig. 2(c) and those in the higher S_{tot}^z sectors are plotted in Fig. 2(d). We find that the short-range staggered spin-spin correlation is decreased with increasing the magnitude of S_{imp}. It may be naturally expected because the AFM fluctuations around higher S_{imp} impurity are suppressed due to weaker quantum fluctuations closer to the classical limit. However, the decay rate of spin-spin correlation for any S_{imp} impurity seems to be comparable to that of the bulk chain, i.e., $\propto r^{-1}$ at short distance ($r \lesssim 100$). We then see an uncommon behavior at larger distance; $C_s(1, j)$ approaches that of the bulk chain at intermediate distance ($100 \lesssim r \lesssim 1000$) and returns to exhibit $C_s(1, j) \propto r^{-1}$ again at large distance ($r \gtrsim 1000$). Although we have confirmed that this uncommon behavior is not an artifact due to finite-size effects by studying several chains with lengths $L = 2000$–4000, the reason why that is so is currently unclear.

In summary, the influence of single impurity on spin-spin correlation is classified broadly into two kinds: (i) $S_{imp} = 0$, 1 with an enhancement of short-range staggered correlation and its decay as $C_s(1, r + 1) \propto r^{-1.5}$, and (ii) $S_{imp} > 1$ with a suppression of short-range staggered correlation and its decay as $C_s(1, r + 1) \propto r^{-1}$.

3. Magnetic impurity with $\Delta_{imp} \neq 1$

Next, we examine how the staggered spin-spin correlation is affected by the XXZ anisotropy (Δ_{imp}) of exchange interaction at magnetic impurity. Figure 3(a) shows DMRG result for $C_s(1, r)$ at several values of Δ_{imp} with $S_{imp} = \frac{1}{2}$ impurity, where the result at $\Delta_{imp} = 1$ is equivalent to that of the bulk SU(2) Heisenberg chain. Since, as discussed below in Sec. III B, the AFM fluctuations around the impurity are sensitive to Δ_{imp}, one may expect a large dependence of $C_s(1, r)$ on Δ_{imp}. However, in fact, the short-range $C_s(1, r)$ is hardly affected by Δ_{imp} and the asymptotic behavior is only slightly changed as $C_s(1, j) \propto r^{-1.05}$ at $\Delta_{imp} = 0$ and $C_s(1, j) \propto r^{-0.95}$ at $\Delta_{imp} = 2$. As shown in Fig. 3(b), DMRG results for the Δ_{imp} dependence of $C_s(2, r)$ with the $S_{imp} = 1$ impurity exhibit qualitatively similar behaviors to those in the case of $S_{imp} = \frac{1}{2}$ impurity. Although the short-range $C_s(2, r)$ is only slightly larger for larger Δ_{imp}, the decay rate at large distance is almost independent of Δ_{imp}, i.e., $C_s(2, r) \propto r^{-1.5}$. This implies that an $S_{imp} = 1$ impurity behaves like a nonmagnetic impurity for any Δ_{imp}. This is another evidence to prove that the valence-bond picture depicted in the inset of Fig. 2(a) is still a good approximation.

Interestingly, as shown in Figs. 3(c)–3(f), the Δ_{imp} dependence of staggered spin-spin correlation functions $C_s(1, r)$ look similar for any $S_{imp} > 1$ impurities. Their qualitative trends are also similar to those for the $S_{imp} = \frac{1}{2}$ impurity; however, the effect of Δ_{imp} seems to be much more

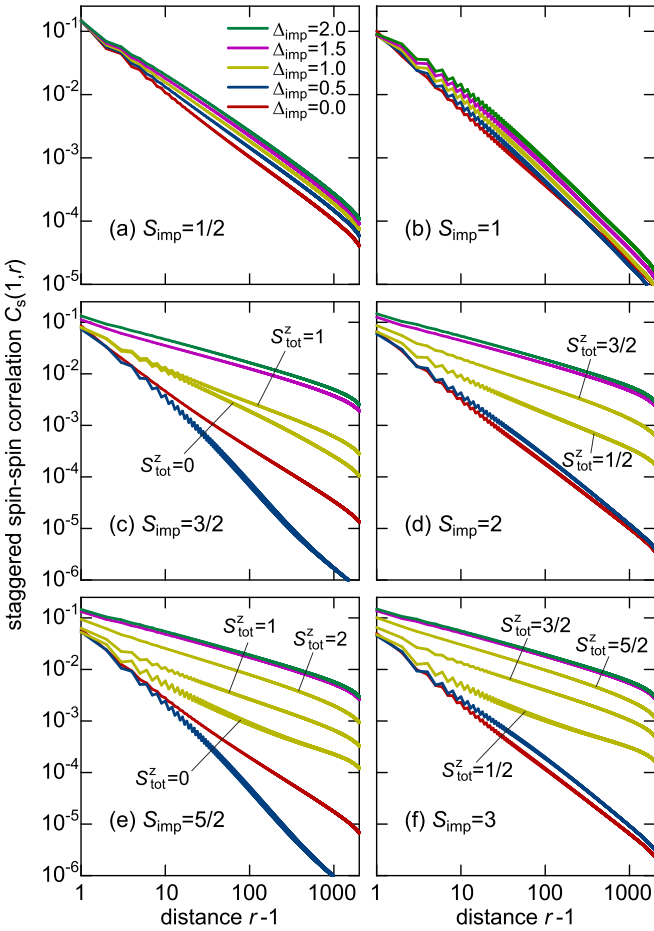FIG. 3. Log-log plots of the staggered spin-spin correlation function $C_s(1, r)$ for (a) $S_{imp} = \frac{1}{2}$, (b) $S_{imp} = 1$, (c) $S_{imp} = \frac{3}{2}$, (d) $S_{imp} = 2$, (e) $S_{imp} = \frac{5}{2}$, and (f) $S_{imp} = 3$ impurities at several Δ_{imp} values. Note that the case of $\Delta_{imp} = 1.0$ in (a) is equivalent to the bulk chain.

FIG. 4. (a)–(c) Expectation values of the z component of local spin $\langle S_i^z \rangle$ in a 200-site SU(2) Heisenberg open chain with an XXZ impurity at the center. (d) Δ_{imp} dependence of $(-1)^i \langle S_i^z \rangle$ around the XXZ impurity.

pronounced. Basically, the decay of $C_s(1, r)$ as a function of r is faster (slower) for smaller (larger) Δ_{imp}. The only exception is that there seems to exist a finite Δ_{imp} which gives the fastest decay of $C_s(1, r)$ for the $S_{imp} = \frac{3}{2}$ and $\frac{5}{2}$ impurities. Note that, for $S_{imp} > 1$ impurities, the DMRG results for all S_{tot}^z sectors giving degenerate ground states are shown.

B. Instability of Néel order with impurities

In the previous subsection, the development of staggered spin-spin correlation on one side of an XXZ magnetic impurity is discussed. Nothing about correlation between spins on both sides of the XXZ magnetic impurity has so far been considered. For example, we know that a nonmagnetic impurity enhances the staggered oscillations on each side of the impurity. However, since the nonmagnetic impurity completely cuts the original SU(2) Heisenberg chain, no correlations exist between the separated chains. One could interpret this to mean that the intrinsic quasi-long-range Néel order in the SU(2) Heisenberg chain is broken by the doping of nonmagnetic impurity. Therefore, we may say that nonmagnetic impurity gives a negative contribution to the stabilization of long-range Néel order.
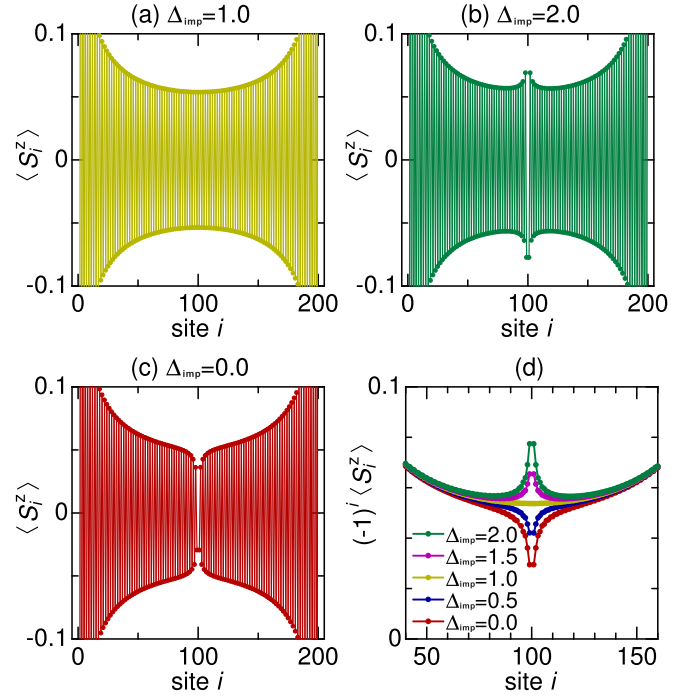
We then investigate how the quasi-long-range Néel order of the SU(2) Heisenberg chain is developed by an XXZ magnetic impurity. We start with an $S_{imp} = \frac{1}{2}$ impurity, where the case of $\Delta_{imp} = 1$ corresponds to no impurity. As a reference state, we prepare quasistaggered order in a 200-site SU(2) Heisenberg open chain, where the z component of edge spins is fixed at $\langle S_1^z \rangle = -\frac{1}{2}$ and $\langle S_{200}^z \rangle = \frac{1}{2}$ in order to control the staggered phase of $\langle S_i^z \rangle$. The spatial distribution of $\langle S_i^z \rangle$ in the reference state, i.e., without impurity, is shown in Fig. 4(a). The staggered oscillation of $\langle S_i^z \rangle$ is created as a consequence of the Friedel oscillation from both chain ends. Despite the decay of $|\langle S_i^z \rangle|$ with $\sim 1/r$ near the both ends [29,30], the amplitude of $|\langle S_i^z \rangle|$ is almost uniform around the center of 200-site chain so that the effect of XXZ magnetic impurity can be clearly demonstrated by replacing the central ($i = 100$) site with the impurity.

It is generally known that the spin-$\frac{1}{2}$ XXZ Heisenberg chain has a long-range Néel order with an easy-axis anisotropy [31–33] and a power-law decay of spin-spin correlation $\langle S_i^z S_{i+r}^z \rangle \sim 1/r^\eta$ ($\eta > 1$) with an easy-plane anisotropy [34,35]. By analogy with this fact, one may naively expect that the Néel stability is enhanced (suppressed) by an XXZ impurity with $\Delta_{imp} > 1$ ($\Delta_{imp} < 1$). In fact, this speculation is confirmed by the enhancement (suppression) of amplitude of $\langle S_i^z \rangle$ around the XXZ magnetic impurity with $\Delta_{imp} = 2$ ($\Delta_{imp} = 0$) as demonstrated in Figs. 4(b) and 4(c). Accordingly, a finite doping of XXZ magnetic impurities with $\Delta_{imp} > 1$ onto an SU(2) Heisenberg chain stabilizes a long-range Néel order since the undoped chain is critical. If we define staggered magnetization, as an order parameter of
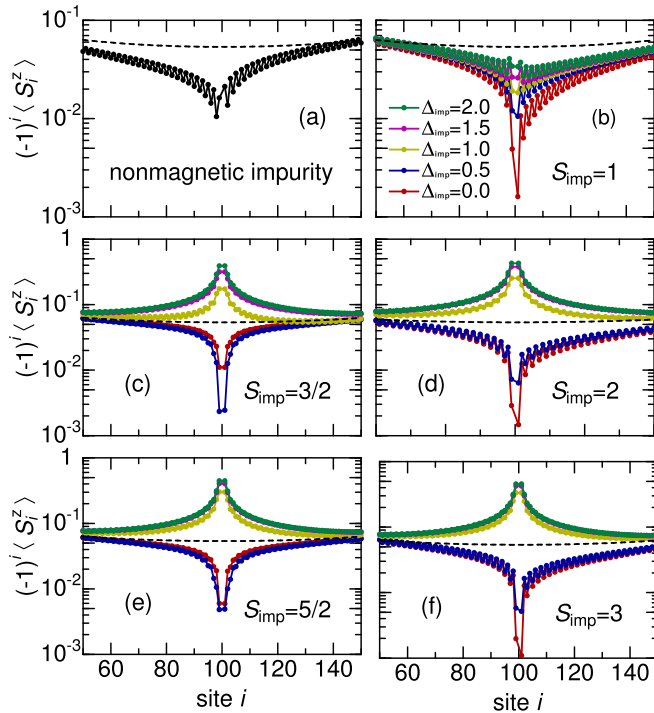
FIG. 5. $\Delta_{\rm imp}$ dependence of staggered z component of local spin around the XXZ magnetic impurity for (a) $S_{\rm imp} = 0$, (b) $S_{\rm imp} = 1$, (c) $S_{\rm imp} = \frac{3}{2}$, (d) $S_{\rm imp} = 2$, (e) $S_{\rm imp} = \frac{5}{2}$, and (f) $S_{\rm imp} = 3$.

the Néel state, by

$$m_{\rm st}^z = \frac{1}{N_c} \sum_1^{N_c} \left| (-1)^i \langle S_i^z \rangle \right|, \qquad (4)$$

$m_{\rm st}^z > 0$ should be achieved for any finite density of XXZ impurities with $\Delta_{\rm imp} > 1$ in the thermodynamic limit. For $n_{\rm imp} = 0$ or $\Delta_{\rm imp} \leqslant 1$, we find $m_{\rm st}^z = 0$ due to lack of long-range Néel order. Details are discussed in Sec. III D. Furthermore, interestingly, the XXZ impurities with $\Delta_{\rm imp} > 1$ would similarly stabilize a long-range Néel order even if the undoped chain is an XXZ Heisenberg chain with easy-plane anisotropy because of the power-law decay of spin-spin correlation in the absence of impurity. To summarize the effect of spin-$\frac{1}{2}$ XXZ impurity on $\langle S_i^z \rangle$, we plot $(-1)^i \langle S_i^z \rangle$ as a function of i for several $\Delta_{\rm imp}$ values in Fig. 4(d). We find that the increase or decrease of amplitude of $\langle S_i^z \rangle$ at the XXZ impurity is roughly proportional to $\Delta_{\rm imp} - 1$.

So, what happens if an SU(2) Heisenberg chain is doped with XXZ impurity other than $S_{\rm imp} = \frac{1}{2}$? To tell the conclusion first, the effects of $S_{\rm imp} > 1$ impurities are qualitatively similar to those in the $S_{\rm imp} = \frac{1}{2}$ case, whereas the nonmagnetic and $S_{\rm imp} = 1$ impurities lead to different behaviors. As done in the case of $S_{\rm imp} = \frac{1}{2}$ impurity, we examine the change of $\langle S_i^z \rangle$ when the central site of 200-site quasi-long-range staggered order is replaced by a nonmagnetic or an XXZ magnetic impurity. Figure 5(a) shows DMRG result for $(-1)^i \langle S_i^z \rangle$ in the case of nonmagnetic impurity. The original staggered oscillation is suppressed around the nonmagnetic impurity because the chain is cut off by the impurity. As expected, a similar behavior is observed in the case of $S_{\rm imp} = 1$ impurity. As seen

in Fig. 5(b), the staggered oscillation is suppressed around the $S_{\rm imp} = 1$ impurity even with large easy-axis anisotropy $\Delta = 2$. This would be a natural consequence of the fact that an $S_{\rm imp} = 1$ XXZ impurity for any $\Delta_{\rm imp}$ acts like a nonmagnetic impurity, as discussed above. Therefore, we conclude that nonmagnetic and $S_{\rm imp} = 1$ impurities only give a negative contribution for the stability of Néel order, namely, $m_{\rm st}^z = 0$ is always obtained when an SU(2) Heisenberg chain is doped with whatever amount of nonmagnetic and $S_{\rm imp} = 1$ impurities.

On the other hand, we find that the original staggered oscillation can be enhanced by $S_{\rm imp} > 1$ impurities if $\Delta_{\rm imp}$ is larger than a certain value $\Delta_{\rm imp,c}$. The results are shown in Figs. 5(c)–5(f). The overall features are similar to those in the case of $S_{\rm imp} = \frac{1}{2}$ impurity. Nevertheless, it is interesting to see that the staggered oscillation is enhanced by the $S_{\rm imp} > 1$ impurities even with isotropic interaction $\Delta_{\rm imp} = 1$ unlike in the case of $S_{\rm imp} = \frac{1}{2}$ impurity. This may be because the higher $S_{\rm imp}$ impurity has a larger Ising anisotropy, due to its classical nature, than the $S_{\rm imp} = \frac{1}{2}$ impurity. The critical values are estimated as $\Delta_{\rm imp,c} = 0.918, 0.997, 0.994,$ and 0.998 for $S_{\rm imp} = \frac{3}{2}, 2, \frac{5}{2},$ and 3 impurities, respectively. Thus, we confirm that a long-range Néel order can be stabilized once an SU(2) Heisenberg chain is doped by $S_{\rm imp} > 1$ impurities with $\Delta \gtrsim 1$.

C. Local spin susceptibility

By studying the local spin susceptibility we can give a theoretical prediction for measured NMR spectra [26,36]. The local spin susceptibility is defined as

$$\chi_i(T) = \frac{1}{T} \sum_j \langle S_i^z S_j^z \rangle, \qquad (5)$$

where T is temperature. Since both the numerator and denominator vanish in the limit of $T \to 0$, we need to transform this, so that we may calculate $\chi_i(T = 0)$. Following Ref. [27], the local spin susceptibility at low temperature is redefined as

$$\chi_i \approx \sum_j \langle \phi_S | S_i^z S_j^z | \phi_S \rangle = S \langle \phi_S | S_i^z | \phi_S \rangle, \qquad (6)$$

where $| \phi_S \rangle$ is the first excited state in the energy spectrum with the z component of total spin $S > 0$. Typically, S is 1 and $\frac{1}{2}$ for a system with an even and odd number of sites, respectively. The local spin susceptibility is a symmetric function under reflections with respect to the center of open system sandwiched by impurities. Since we find only staggered oscillations of S_i^z in the all cases, χ_i can be divided into a "uniform" component $\chi_i^{\rm u}$ and "staggered" component $\chi_i^{\rm a}$ using the definition $\chi_i = \chi_i^{\rm u} - (-1)^i \chi_i^{\rm a}$. The uniform and staggered components are practically obtained as $\chi_i^{\rm u} = \chi_i/2 + (\chi_{i-1} + \chi_{i+1})/4$ and $\chi_i^{\rm a} = -(-1)^i(\chi_i - \chi_i^{\rm u})$, respectively.

In Figs. 6(a) and 6(b), DMRG results for the uniform and staggered components of local spin susceptibility using simple open chains with 49 and 50 sites are shown. The open chains are regarded as chain segments created by doping of nonmagnetic impuritues into an SU(2) Heisenberg chain. The staggered component $\chi_i^{\rm a}$ is forced to be symmetric for odd L and antisymmetric for even L as a consequence of finite-size
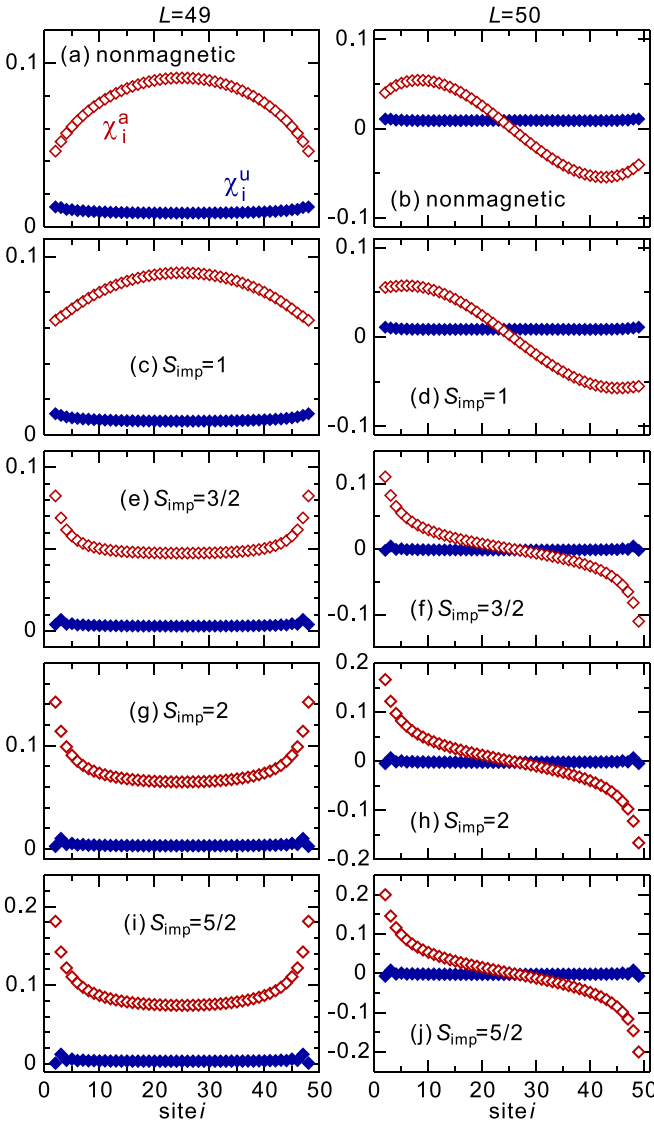
FIG. 6. Uniform and staggered components of the local susceptibility χ_i for (a) $S_{\mathrm{imp}} = 0$, (b) $S_{\mathrm{imp}} = 1$, (c) $S_{\mathrm{imp}} = \frac{3}{2}$, (d) $S_{\mathrm{imp}} = 2$, (e) $S_{\mathrm{imp}} = \frac{5}{2}$, and (f) $S_{\mathrm{imp}} = 3$, obtained with spin-$\frac{1}{2}$ chain segments with 49 (left panel) and 50 sites (right panel).

FIG. 7. Δ_{imp} dependence of staggered component of the local susceptibility χ_i for (a) $S_{\mathrm{imp}} = 1$, (b) $S_{\mathrm{imp}} = \frac{3}{2}$, (c) $S_{\mathrm{imp}} = 2$, and (d) $S_{\mathrm{imp}} = \frac{5}{2}$ impurities. The system length is $L = 49$.

effect. As consistent with Ref. [27], the maximum position of χ_i^{a} is distant as much as possible from the chain ends. This is also consistent with the prediction that χ_i^{a} simply increases as a function of distance from the nonmagnetic impurity for a semi-infinite chain [26].

Let us then consider the case of magnetic impurity. We first focus on the cases of $\Delta_{\mathrm{imp}} = 1$. For this, we need to prepare SU(2) chain segment with impurities at both ends. We here create such a chain segment by replacing two opposite sites on an SU(2) periodic chain with two magnetic impurities. Specifically, periodic SU(2) chains with 100 and 102 sites are used to configure chain segments with 49 and 50 sites, respectively. Figures 6(c) and 6(d) show DMRG results for χ_i^{u} and χ_i^{a} in the case of $S_{\mathrm{imp}} = 1$ impurity. As might be expected from the above discussions, they are even quantitatively similar to those in the case of nonmagnetic impurity. This is another evidence to prove that an $S_{\mathrm{imp}} = 1$ impurity behaves like a nonmagnetic
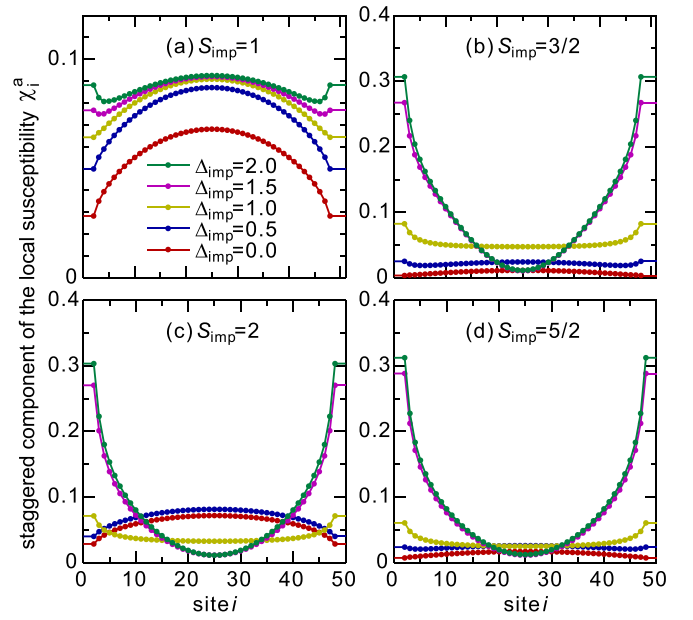
impurity. On the other hand, the local spin susceptibility for $S_{\mathrm{imp}} > 1$ impurities exhibits substantially different features as shown in Figs. 6(e)–6(j). The results for χ_i^{u} and χ_i^{a} in the cases of $S_{\mathrm{imp}} = \frac{3}{2}$, 2, and $\frac{5}{2}$ impurities look qualitatively similar. For both system sizes, χ_i^{a} has a maximum value near the magnetic impurities. To illustrate the spin state around the magnetic impurity, as an example, let us consider the three-spin Heisenberg problem; an $S = \frac{3}{2}$ with two adjacent $S = \frac{1}{2}$'s. The dominant configuration of the ground state in the $S^z = \frac{1}{2}$ sector is expressed as

$$\psi \approx \left| \frac{1}{2}, -\frac{1}{2} \right\rangle \otimes \left| \frac{3}{2}, \frac{3}{2} \right\rangle \otimes \left| \frac{1}{2}, -\frac{1}{2} \right\rangle. \qquad (7)$$

Since the $S = \frac{1}{2}$ states tend to localize at the $S_{\mathrm{imp}} = \frac{3}{2}$ impurity, it leads to the maximum value of $|\chi_i^{\mathrm{a}}|$ near the $S_{\mathrm{imp}} = \frac{3}{2}$ impurity. Nevertheless, χ_i^{a} for $L = 49$ reduces to a finite saturated value with the distance from the $S_{\mathrm{imp}} = \frac{3}{2}$ impurity. This means that the localization of $S = \frac{1}{2}$ states near the $S_{\mathrm{imp}} > 1$ impurities is not very strong. These trends are also seen in the case of $S_{\mathrm{imp}} > 0$ impurities. The exact solution of three-spin Heisenberg problem for $S_{\mathrm{imp}} > 0$ impurities is given in Appendix A.

We further investigate the Δ_{imp} dependence of χ_i^{a}. Figure 7(a) shows DMRG results for χ_i^{a} at several Δ_{imp} values in the case of $S_{\mathrm{imp}} = 1$ impurity. The overall trends almost remain unchanged with Δ_{imp} although χ_i^{a} is broadly enhanced (suppressed) with increasing (decreasing) Δ_{imp}. This may be naively expected from the fact that $S_{\mathrm{imp}} = 1$ impurity behaves like nonmagnetic impurity for any Δ_{imp}. On the other hand, as shown in Figs. 7(b)–7(d), χ_i^{a} for $S_{\mathrm{imp}} > 1$ impurities is significantly affected by Δ_{imp}. With increasing Δ_{imp}, χ_i^{a} near the magnetic impurity is markedly enhanced and it becomes very small at the middle of chain. This is interpreted to mean
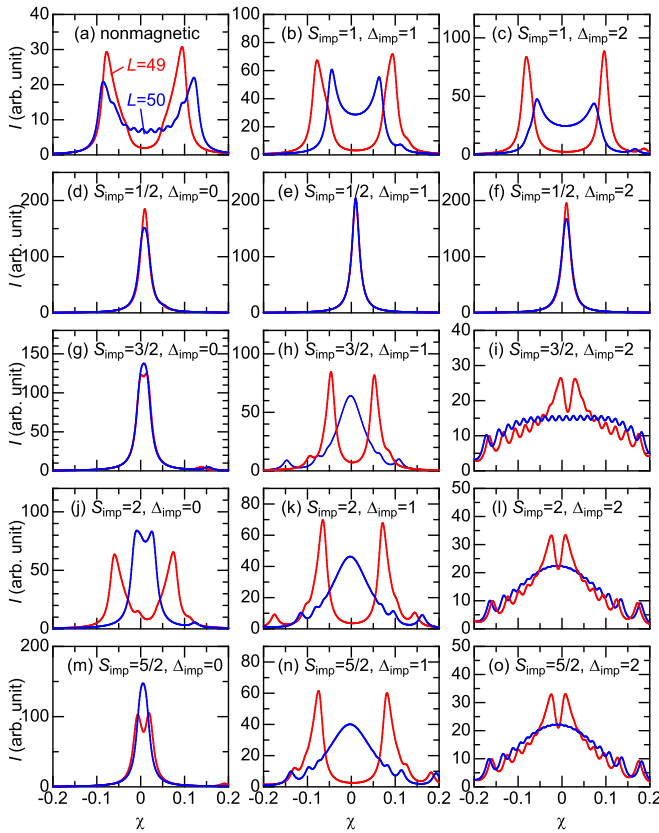
FIG. 8. Δ_{imp} dependence of NMR spectra for (a) $S_{\mathrm{imp}} = 0$, (b), (c) $S_{\mathrm{imp}} = 1$, (d)–(f) $S_{\mathrm{imp}} = \frac{1}{2}$, (g)–(i) $S_{\mathrm{imp}} = \frac{3}{2}$, (j)–(l) $S_{\mathrm{imp}} = 2$, and (m)–(o) $S_{\mathrm{imp}} = \frac{5}{2}$ impurities. A Lorentzian broadening 0.01 is introduced.

that the $S = \frac{1}{2}$ states are strongly localized near the $S_{\mathrm{imp}} > 1$ impurity because the state denoted by Eq. (7) becomes progressively more dominant for larger Δ_{imp}. While at small $\Delta_{\mathrm{imp}} < 1$ the localization of $S = \frac{1}{2}$ states near the magnetic impurity is weakened (also see Appendix A), χ_i^a has its maximum at the middle of chain like in the cases of nonmagnetic and $S_{\mathrm{imp}} = 1$ impurities. This effect is most pronounced in the case of $S_{\mathrm{imp}} = 2$. Incidentally, in the case of $S_{\mathrm{imp}} = \frac{1}{2}$ impurity, the local spin susceptibility is always very small for $0 < \Delta_{\mathrm{imp}} < 5$ and thus $|\chi_i^a| \lesssim 0.01$.

Once the staggered component of the local susceptibility is calculated, it would be interesting to see its amplitude distribution, which can be detected as a broadening of the NMR spectra [26,36]. A Lorentzian broadening 0.01 is introduced to obtain the NMR spectra. Figures 8(a)–8(c) show the NMR spectra for nonmagnetic and $S_{\mathrm{imp}} = 1$ impurities. In these cases, we find a two-peak structure, where the distance between peaks roughly corresponds to an amplitude of χ_i because the maximum position of χ_i^a moves away from the impurities due to the delocalized character of spinon excitation. For the $S_{\mathrm{imp}} = \frac{1}{2}$ impurity, as shown in Figs. 8(d)–8(f), the NMR spectra always consist of a single sharp peak because of $|\chi_i^a| \lesssim 0.01$ for any Δ_{imp}.

Based on the results for χ_i^a, a strong dependence of NMR spectra on Δ_{imp} is expected for $S_{\mathrm{imp}} > 1$ impurities. The NMR spectra for $S_{\mathrm{imp}} = \frac{3}{2}$, 2, and $\frac{5}{2}$ impurities are shown in Figs. 8(g)–8(o). The results in these three cases are qual-

itatively similar: At $\Delta_{\mathrm{imp}} = 1$ the NMR spectra for $L = 50$ exhibit a broad peak centered at zero, reflecting a weak localization of the $S = \frac{1}{2}$ states near the magnetic impurities. At $\Delta_{\mathrm{imp}} = 2$ the localization of $S = \frac{1}{2}$ states near the magnetic impurities is strongly enhanced and the NMR spectra become much broader. At $\Delta_{\mathrm{imp}} = 0$ the NMR spectra show a rather narrow peak because the amplitude of χ_i^a is very small like in the case of $S_{\mathrm{imp}} = \frac{1}{2}$ impurity.

We then analyze the experimental NMR spectra of the Co-doped $SrCuO_2$ compound $SrCu_{0.99}Co_{0.01}O_2$ [19]. A very broad peak with a central small dip was experimentally observed at low temperature. A remaining issue is that the spin state of Co ion, which is either $S = \frac{3}{2}$ or $\frac{1}{2}$, has not been identified up to now. We could find an answer to this question, although the results for $L = 49$ and 50 may reveal typical features of $\sim 2\%$ doping and we need to take an average over L using Eq. (2) with $n_{\mathrm{imp}} = 0.01$ for quantitative analysis. We argue that the low-temperature broad NMR spectra $SrCu_{0.99}Co_{0.01}O_2$ can be explained only when the spin state of Co ion is assumed to be $S = \frac{3}{2}$ and the spin anisotropy to be $\Delta_{\mathrm{imp}} > 1$.

D. Staggered magnetization with finite impurity doping

Let us then investigate the staggered magnetization m_{st}^z, defined by Eq. (4), as functions of the XXZ anisotropy Δ_{imp} and impurity density n_{imp}. As mentioned above, the effect of magnetic impurity on the stability of Néel order in the SU(2) Heisenberg chain can be classified broadly into two types: One is nonmagnetic and $S_{\mathrm{imp}} = 1$ impurities which simply suppress the Néel stability and the other is $S_{\mathrm{imp}} = \frac{1}{2}$ and $S_{\mathrm{imp}} > 1$ impurities which encourage the development of long-range Néel order if $\Delta_{\mathrm{imp}} \gtrsim 1$. Thus, it would be reasonable to consider the case of $S_{\mathrm{imp}} = \frac{1}{2}$ as a representative of the latter although there may be quantitative differences from the case of $S_{\mathrm{imp}} > 1$. Therefore, we focus on the case of $S_{\mathrm{imp}} = \frac{1}{2}$ impurity hereafter.

When an SU(2) Heisenberg chain is doped with an $S_{\mathrm{imp}} = \frac{1}{2}$ impurity with $\Delta_{\mathrm{imp}} > 1$, a staggered oscillation of $\langle S_i^z \rangle$ may be induced as a Friedel oscillation from the impurity. The amplitude of this Friedel oscillation decays as $\langle S_r^z \rangle \sim 1/r^\eta$ since it mimics the decay of spin-spin correlation function of the SU(2) Heisenberg chain [37]. The value of η can be estimated to be ~ 1 from the slope of $C_s(1, r)$ in Fig. 3(a). This means that, if the SU(2) chain is doped with more than one impurity, the staggered oscillation reaches the next impurity with maintaining its amplitude of the order of $C_s(1, 1)/\bar{l} \approx 0.2 n_{\mathrm{imp}}/(1 - n_{\mathrm{imp}})$. As shown in Fig. 4(d), this staggered oscillation is further enhanced at the next impurity. Therefore, $m_{\mathrm{st}}^z > 0$ is naively expected as long as $n_{\mathrm{imp}} > 0$ and $\Delta_{\mathrm{imp}} > 1$. In other words, the presence of finite amount of XXZ impurities with $\Delta_{\mathrm{imp}} > 1$ induces a long-range Néel order in the doped SU(2) Heisenberg chain. In order to numerically confirm it, we calculate m_{st}^z for various sets of Δ_{imp} and n_{imp} using DMRG method. We study open chains with length $N_c = 40$–800. For a given length N_c, the value of m_{st}^z is obtained by averaging over $10\,000/N_c$ samples, and then a finite-size scaling analysis to the thermodynamic limit $N_c \to \infty$ is performed. In Fig. 9(a), the obtained values of m_{st}^z are
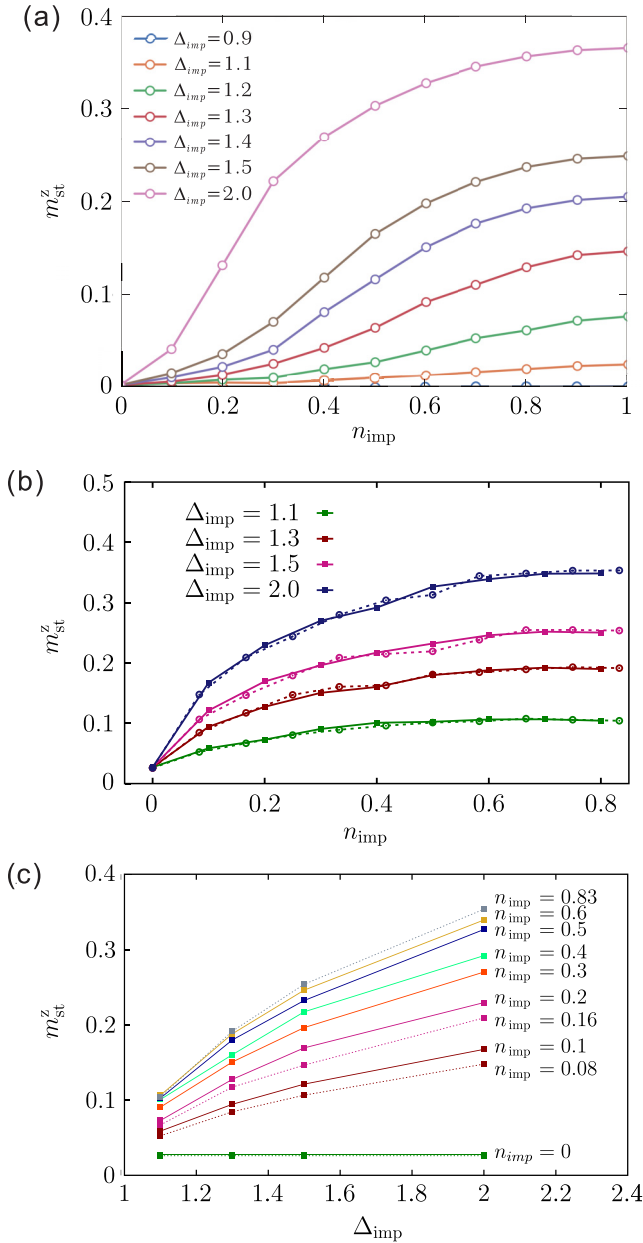
FIG. 9. Variation of staggered magnetization m_z^{st} with impurity density n_{imp} for different values of anisotropy (Δ_{imp}) with using (a) DMRG and (b) CMFT approaches. (c) CMFT results for m_z^{st} as a function of Δ_{imp} at fixed values of n_{imp}. In (b) and (c), the solid and dashed lines correspond to the CMFT results for $N_c = 10$ and 12, respectively.

plotted as a function of n_{imp} for several values of Δ_{imp}. We find that m_{st}^z is always finite for $n_{imp} > 0$ and $\Delta_{imp} > 1$. The qualitative trend of m_{st}^z vs n_{imp} is common for any $\Delta_{imp}(> 1)$; it is small at low n_{imp}, increases rapidly at some intermediate n_{imp}, and saturates to a value at high n_{imp}. The saturation value agrees perfectly with spontaneous magnetization of the XXZ Heisenberg chain [32,33]. For a fixed $n_{imp}(> 0)$, m_{st}^z increases with increasing Δ_{imp}. This is a natural consequence of the fact that the amplitude of induced staggered oscillation is larger for larger Δ_{imp}. It is interesting that the largest slope of $\partial m_{st}^z / \partial n_{imp}$ is given by smaller n_{imp} for larger Δ_{imp}.

We also estimate m_{st}^z using CMFT, which may provide a crosscheck for the above DMRG results. The ground state of an AFM spin chain as obtained by CMFT is a mixed state forming valence bonds on alternate sites in the presence of very small yet finite (less than 10% of the spin magnitude) staggered magnetization. The presence of an impurity introduces Δ_{imp} in the bonds connecting the impurity. In Fig. 9(b), we show the CMFT results for variation of m_{st}^z with n_{imp} for $N_c = 10$ (solid lines), and 12 (dashed lines) averaged over 20 random configurations. For a particular Δ_{imp}, increase in the number of anisotropic bonds increases m_{st}^z, indicating the formation of stronger Néel order. It is interesting to note that anisotropic strength as low as $n_{imp} = 0.1$ can induce an ordered state. Since calculations performed on larger cluster size of $N_c = 12$ (dashed lines) do not show any qualitative difference in the results, most of the analysis will be restricted to a cluster of 10 sites.

Figure 9(c) shows the evolution of m_{st}^z for different n_{imp} with increasing Δ_{imp}. It suggests that introducing a single impurity spin ($n_{imp} = 0.1$ in a spin chain of $N_c = 10$ and $n_{imp} = 0.08$ in a spin chain of $N_c = 12$) affects the overall order of the chain. This effect can be further increased by increasing Δ_{imp}. Note that configurations do not include edge spins so MF bonds are always pure. It is interesting to observe that staggered magnetization increases (decreases) with increasing (decreasing) the cluster size since this sampling underestimates (overestimates) magnetization for lower (higher) impurity density. Detailed discussion on the number of random samplings is given in Appendix C. While the qualitative behavior of m_{st}^z calculated using CMFT matches very well with that obtained via DMRG, results obtained using CMFT suffer from finite-size mean-field effects. The finite-size effect leads to higher m_{st}^z in comparison to DMRG. This effect is more pronounced for small n_{imp}, as for low n_{imp} the number of Heisenberg bonds is larger and CMFT breaks the rotational symmetry of the Hamiltonian. CMFT results can be further improved by increasing the cluster size. Detailed discussion on the finite-size effect is given in Appendix D.

E. Uniform magnetization with external field

In this section, we discuss the Δ_{imp} and n_{imp} dependence of total magnetization in the presence of external field h_z. The total magnetization is defined by

$$m^z = \frac{1}{L} \sum_1^L \langle S_i^z \rangle. \tag{8}$$

We begin by discussing the behavior of uniform magnetization m^z of pure XXZ Heisenberg chain with exchange anisotropy Δ as a function of h_z. The Hamiltonian reads as $\mathcal{H} = \sum_i [(S_i^+ S_{i+1}^- + S_i^- S_{i+1}^+)/2 + \Delta S_i^z S_{i+1}^z] + h_z \sum_i S_i^z$. The DMRG results for m^z are plotted in Fig. 10(a). For $\Delta \leqslant 1$, with increasing h_z, m^z increases almost linearly at low h_z and exhibits a divergent saturation reflecting the strong quantum fluctuations. For $\Delta > 1$, m^z remains zero up to a finite $h_z (\equiv h_{z,cr})$ because of the long-range Néel order, it rises up vertically at $h_z = h_{z,cr}$, and at higher h_z behavior is qualitatively similar to that for $\Delta \leqslant 1$. The saturation field is $h_{sat} = 1 + \Delta$ for any Δ. We then investigate
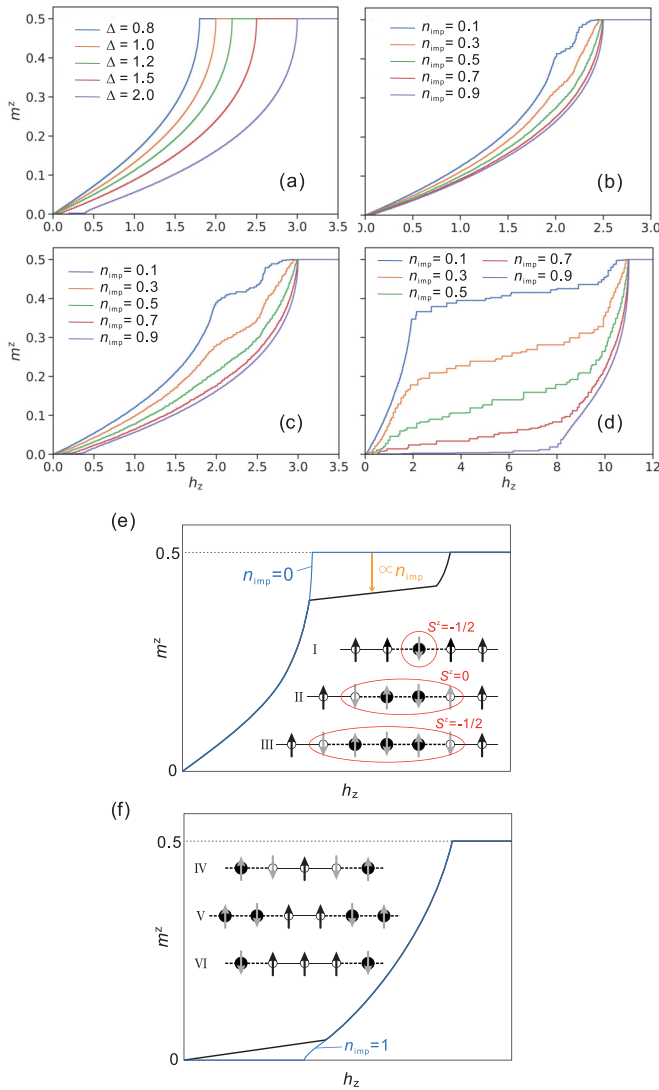
FIG. 10. (a) Magnetization curve of XXZ Heisenberg chain as a function of magnetic field h_z. (b)–(d) Magnetization curves of doped SU(2) Heisenberg chain by $S_{imp} = \frac{1}{2}$ XXZ impurities with (b) $\Delta_{imp} = 1.5$, (c) 2, and (d) 10 for several impurity densities n_{imp}. (e), (f) Schematic illustrations of magnetization curve near (e) $n_{imp} = 0$ and (f) $n_{imp} = 1$. The insets of (e) [(f)] show schematic representations of typical spin states near $n_{imp} = 0$ at high fields ($n_{imp} = 1$ at low fields), where the solid line denotes spin-isotropic XXX bond and the dashed line denotes spin-anisotropic XXZ bond.

the n_{imp} dependence of magnetization curve for doped SU(2) Heisenberg chain by XXZ anisotropic $S_{imp} = \frac{1}{2}$ impurities with Δ_{imp}. In other words, we see how the magnetization curve is varied from that of $\Delta = 1$ to that of $\Delta = \Delta_{imp}$ with increasing n_{imp}.

In Figs. 10(b)–10(d), DMRG results for the magnetization curve with $\Delta_{imp} = 1.5$, 2, and 10 at several values of n_{imp} are shown. The undoped system is an SU(2) Heisenberg chain. For each curve shown in Figs. 10(b)–10(d), m^z is calculated by taking average over 10 random realizations of impurity distributions on an open chain of length $N_c = 1000$. Qualitatively, the n_{imp} dependence of m^z vs h_z is similar for all Δ_{imp} cases. Nevertheless, the characteristics become more obvious with

larger Δ_{imp}. The specific features can be interpreted by the fact that XXX spins are more easily polarized than XXZ spins with easy-axis anisotropy ($\Delta_{imp} > 1$).

At low impurity density ($n_{imp} \sim 0$), a plateaulike feature is seen near the saturation $m^z \sim \frac{1}{2}$. If the impurities are dilute, the system consists of field-polarized spins and isolated magnons at high fields because the XXZ impurity spins are initially flipped with decreasing field from the saturation. This spin state is sketched as I in the inset of Fig. 10(e). Since there is a "gap" between field strengths to polarize the XXZ impurity spins and the other spins, a plateau is created at $m^z \approx (1 - n_{imp})/2$. As n_{imp} increases, the probability that two or more XXZ impurities are aligned increases in the h_z range of plateau. For example, when two XXZ impurities are placed next to each other, as II in the inset of Fig. 10(e), a tetramer singlet ($S^z = 0$) is composed of four spins connected by XXZ coupling (we call a chain segment like the tetramer in this case "XXZ chain segment"). Thus, a finite gap to $S^z = 1$ takes the shape of plateau. Similarly, when three XXZ impurities are aligned, a pentamer is formed as III in the inset of Fig. 10(e). Having polarized spins on either side of the pentamer, a gap opens between $S^z = -\frac{1}{2}$ and $\frac{1}{2}$ states. It also creates a plateau. In general, an XXZ chain segment with even (odd) number of XXZ impurities exhibits a gap between $S^z = 0$ and 1 states ($S^z = -\frac{1}{2}$ and $\frac{1}{2}$ states). Since the gap value differs by the length of XXZ chain segment, the plateau has a finite slope. Basically, odd-length XXZ chain segments have larger gap than even-length ones; the gap is larger for shorter XXZ chain segment. The more various lengths of XXZ chain segments exist, the more the slope of plateau becomes steep. Indeed, the increase of slope with increasing n_{imp} can be confirmed up to $n_{imp} = 0.3$ in Figs. 10(b)–10(d).

At high impurity density ($n_{imp} \sim 1$) the overall shape of m^z vs h_z looks similar to that of XXZ Heisenberg chains with $\Delta = \Delta_{imp}$ because most parts of the system are covered by XXZ chain segments with Δ_{imp}. However, a slow increase of m^z is seen at lower h_z instead of gapped behavior in the XXZ Heisenberg chain. This is caused by a scattering of undoped XXX chain segments, as sketched in the inset of Fig. 10(f). The XXX chain segments are more easily polarized than XXZ chain segments. Since typical field strengths exhibiting the states IV, V, and VI are different, i.e., $h_z(VI) > h_z(V) > h_z(IV)$, a gradual slope of m^z at lower h_z is created.

It would be informative to compare CMFT results for the uniform magnetization m^z with those by DMRG. In Fig. 11, we show CMFT results for m^z as a function of applied magnetic field for different values of impurity densities. Similar to the DMRG results, for $n_{imp} = 0$, total magnetization continuously increases with applied field until saturation where all the spins align in the direction of field [see Fig. 11(a)]. Small steplike features obtained in net magnetization is a consequence of finite-size effects in CMFT, which can be reduced with increasing cluster size. Numerically exact results obtained from DMRG begin from zero magnetization owing to the gapless nature of 1D Heisenberg AFM and continuously increases until saturation field. While the intermediate behavior of m^z obtained by CMFT does not match with the results of DMRG, it is interesting to note that the value of saturation field agrees very well.
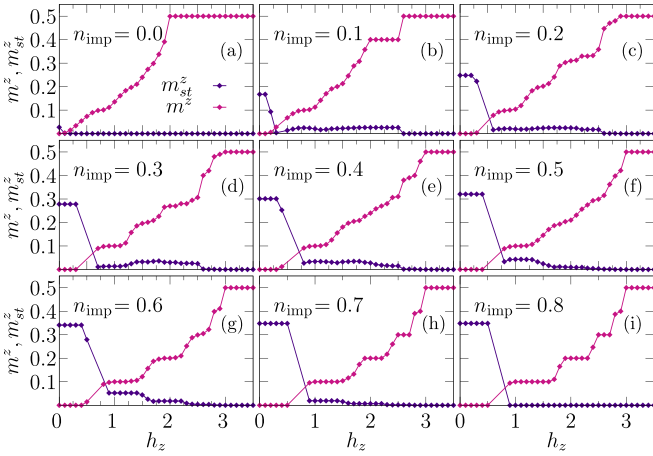
FIG. 11. Variations of total magnetization m^z (pink) and staggered magnetization m^z_{st} (purple) with increasing applied magnetic field for different values of n_{imp} as indicated in the panels. Δ is fixed to 2 and N_{av} is set to 10.

In Figs. 11(b)–11(i) we show the variation of total magnetization m^z (pink) and staggered magnetization m^z_{st} (purple) with increasing applied magnetic field for different values of n_{imp} as indicated in the panels. A Néel order is formed on substitution of impurities, which vanishes above a finite magnetic field. This critical value of the field above which Néel order vanishes increases with increase in n_{imp}. This is understood as the closing of the gap existing above the ground state. This feature is reflected in m^z remaining zero up to a finite strength of magnetic field that is equal to the energy gap above the ground state. In the XXZ limit, this gap is related to the anisotropy in Hamiltonian [38,39]. Note that results for some field values are omitted as for those applied field values, mean fields did not converge for some random configurations. It is interesting as mean fields converged for all other values of applied field with the same set of random configurations. Further increase in the impurity density increases the saturation magnetic field strength. For the extreme case, when $n_{imp} = 0.8$, all the bonds except mean-field decoupled ones are anisotropic in nature. Disregarding the field values of nonconvergence, the behavior of net magnetization and staggered magnetization reveals formation of Néel order in low fields and fully saturated state in high-field limit. The results for m^z with applied field match with those obtained in $BaCo_2V_2O_8$ [40]. This material is expected to be explained by a quasi-1D XXZ model with $\Delta_{imp} = 2$. An ideal XXZ chain model will show a quantum phase transition from the Néel ordered phase to Tomonaga-Luttinger liquid to saturated state at high fields. Further investigations are required to understand this intermediate order appearing in the presence of field using CMFT.

IV. THERMODYNAMIC PROPERTIES

In the previous section, we have established that the antiferromagnetic order is induced in an isotropic spin chain on substitution of a spin-$\frac{1}{2}$ magnetic impurity resulting in anisotropic neighboring bonds. We now discuss signatures of phase transition appearing in specific heat (C_v) and suscepti-
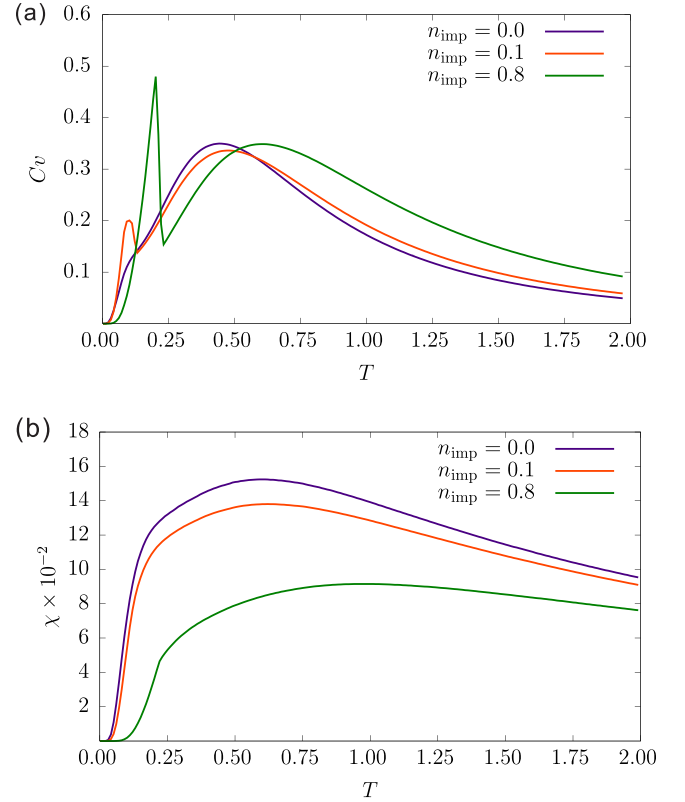

FIG. 12. CMFT results for variation of (a) specific heat and (b) susceptibility with temperature for different values of impurity density while the anisotropy strength is fixed to $\Delta_{imp} = 2$.

bility (χ) with increasing temperature for different values of impurity density n_{imp} and Δ_{imp}.

Figure 12(a) shows variation of C_v with temperature for different n_{imp} with $\Delta_{imp} = 2$. For a completely isotropic spin chain ($n_{imp} = 0$), specific heat changes smoothly with broadened peak near $T = 0.4$. For impurity density as low as $n_{imp} = 0.1$, a small peak emerges as a consequence of phase transition from a Néel phase to a paramagnet. The peak in C_v sharpens when n_{imp} increases. The huge bump in C_v for higher temperature is a consequence of continuously decreasing correlations among spins. The origin of this behavior is discussed in detail in Sec. III E. Figure 12(b) shows that χ decreases with increase in impurity density. Results for susceptibility in the completely Heisenberg limit show an unusual curvature in $T < 0.25$, which differs from the behavior expected from the ideal 1D antiferromagnetic Heisenberg chain. The result shown here is a consequence of the mixed Néel order with dimer correlations as obtained using CMFT. The susceptibility matches with the one expected from an alternating exchange antiferromagnetic chain (weakly coupled dimers) [41]. A significant deviation appears for high n_{imp} in lower-temperature region while the behavior qualitatively remains the same in higher-T limit.

In Fig. 13, we show the dependence of Δ_{imp} on specific heat and susceptibility for different impurity densities. Results for specific heat reveal that the increase in the anisotropy strength (Δ_{imp}) increases the transition temperature as well as the specific-heat peak. This effect is consistent for all
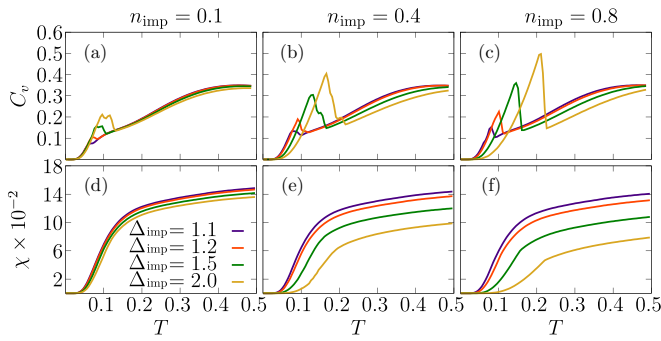
FIG. 13. Variations of specific heat and susceptibility for different values of Δ_{imp}. The results are obtained for (a), (d) $n_{imp} = 0.1$, (b), (e) $n_{imp} = 0.4$, and (c), (f) $n_{imp} = 0.8$.

FIG. 15. Variations of susceptibility with temperature obtained using CMFT on a cluster size consisting of 10 spins ($\Delta_{imp} = 2.0$). Dependence on n_{imp} is shown for various number of random configurations: $N_{av} = 10$ (yellow), 20 (blue), and 40 (red).

impurity densities $n_{imp} = 0.1$, 0.4, and 0.8 as shown in Figs. 13(a)–13(c). Results for the susceptibility in completely isotropic case ($n_{imp} = 0$) calculated using CMFT are similar to that of χ obtained for antiferromagnetic dimer chain [41]. For $n_{imp} = 0.1$, no significant change in susceptibility is identified on increasing Δ_{imp}. Further increase in impurity density leads to decrease in χ, which is prominent for higher Δ_{imp}.

Presence of impurity bonds induces a Néel order, which melts to a disordered state with increase in temperature. As this effect is more significant in low-temperature regime, Figs. 14 and 15 show the variations of C_v and χ with temperature for different n_{imp} with fixed $\Delta_{imp} = 2.0$. Transition temperature increases with increase in n_{imp}. Although the effect of interchain coupling is taken into account as mean field in this paper, this trend would remain correct even if the interchain couplings are explicitly included in the system. For high n_{imp}, the peak in specific heat is very sharp owing to the Ising-type nature of most of the bonds. For intermediate values of impurity densities, the number of possible random distributions of the impure spins is huge, leading to difference in magnetic order. Different colors in Fig. 14 correspond to different N_{av}. For intermediate values of n_{imp}, specific heat

shows a broad peak, which becomes smooth with further increase in N_{av}. Nonmonotonic behavior in C_v for intermediate n_{imp} is a direct consequence of the distribution of impure spins. We believe that these peculiarities might be a finite-size effect and will lead to a clear phase transition in the thermodynamic limit.

Figure 15 shows dependence of χ with increasing the number of random configurations used for averaging. It is interesting to note that susceptibility decreases with increase in impurity density. Impurity effects in susceptibility are more prevalent for higher n_{imp}, where it shows a discontinuity at $T \sim 0.25$ [see Figs. 15(g)–15(i)]. Results for susceptibility of SrCo$_2$V$_2$O$_8$ [18] show a signature similar to χ obtained for higher n_{imp}. SrCo$_2$V$_2$O$_8$ is expected to be described by the XXZ model; however, interchain interactions induce an order in the material at low temperatures. The discontinuity identified in χ is a result of vanishing Nèel order.

V. CONCLUSION

Using DMRG and CMFT, we studied an AFM spin-$\frac{1}{2}$ Heisenberg chain doped with spin-S XXZ magnetic impurities, where an XXZ anisotropic impurity Δ_{imp} introduces XXZ exchange interaction in the neighboring bonds. First, we examined the effect of a single spin-S XXZ magnetic impurity in the ground-state properties such as the spin-spin correlation function, instability of Néel order, and local spin susceptibility. Based on their qualitative characteristics we find that the types of spin-S impurities are classified into two groups. (i) One contains nonmagnetic and $S = 1$ impurities. A short-range AFM correlation is enhanced but the decay rate of spin-spin correlation function is faster than that of the undoped spin-$\frac{1}{2}$ Heisenberg chain. Since they behave like a magnetic defect, i.e., vacancy, the global Néel order cannot be supported. (ii) The other contains $S = \frac{1}{2}$ and $S > 1$ impurities. They hardly change the decay rate of spin-spin correlation function. However, the Néel fluctuation is significantly enhanced around the easy-axis XXZ anisotropic impurities in the spin-$\frac{1}{2}$ Heisenberg chain, so that long-range Néel order
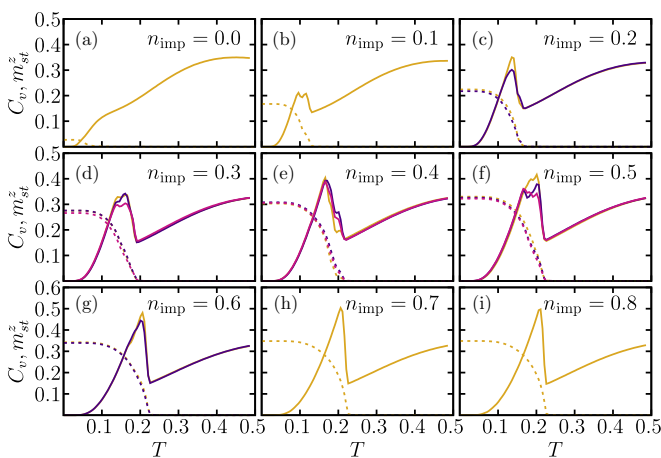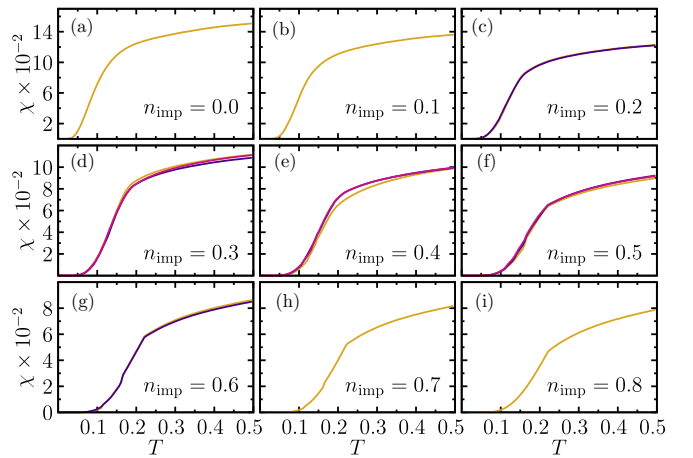

FIG. 14. Variations of specific heat (solid lines) and staggered magnetization (dashed lines) with temperature obtained using CMFT on a cluster size consisting of 10 spins. Dependence on n_{imp} is shown for various number of random configurations: $N_{av} = 10$ (yellow), 20 (blue), and 40 (red).

can obviously be stabilized. We also found that the experimentally observed broad NMR spectra at low temperature in $SrCu_{0.99}Co_{0.01}O_2$ may be a consequence of the presence of large Δ_{imp}, $S = \frac{3}{2}$ impurities.

In the latter part of this paper, we focused on the case of $S = \frac{1}{2}$ impurity as a representative of (ii). By considering the staggered magnetization m_{st}^z as an order parameter of the Néel state, we confirmed that a finite amount of easy-axis XXZ $S = \frac{1}{2}$ impurities immediately induces a Néel order in the bulk spin chain and m_{st}^z increases with increasing Δ_{imp} and n_{imp}. In the presence of uniform magnetic field h_z, the total magnetization m^z exhibits a pseudogap behavior at low h_z, which is more pronounced when approaching a pure easy-axis XXZ Heisenberg chain in the $n_{imp} = 1$ limit. Also, a plateaulike feature at $m^z \sim (1 - n_{imp})/2$ revealing the existence of isolated magnons is seen at low n_{imp}.

Furthermore, we investigated the thermodynamic properties such as specific heat and magnetic susceptibility using CMFT. These calculations revealed a phase transition from a Néel order to a paramagnet. The transition temperature as well as the size of the peak in specific heat increases with increase in n_{imp} and Δ_{imp}. The dependence of the transition temperature on the concentration and anisotropy strength of impurities is relevant for real systems, where finite-temperature phase transitions become possible due to interchain couplings.

It is also worth noting that the effect of spin-S impurities on ferromagnetic chain is a nontrivial question. Very recently, the interaction-induced bound magnon edge state, which may behave like a spin-S impurity, in anisotropic ferromagnetic chain was studied [42]. The extension of our study to ferromagnetic chain is expected in the future.

APPENDIX A: LOCALIZED $S = \frac{1}{2}$ STATES NEAR $S_{imp} > 1$ IMPURITY

In Sec. III C, we argue that the $S = \frac{1}{2}$ states are localized around the $S_{imp} > 1$ impurity in the $S^z = \frac{1}{2}$ sector. To explain this, we consider a simplified three-site Heisenberg system consisting of an $S_{imp} = T/2$ impurity and the neighboring two $S = \frac{1}{2}$'s. In the $S^z = \frac{1}{2}$ sector, possible bases are

$$\phi_1 = \left| \frac{1}{2}, \frac{1}{2} \right\rangle \otimes \left| \frac{T}{2}, -\frac{1}{2} \right\rangle \otimes \left| \frac{1}{2}, \frac{1}{2} \right\rangle, \quad (A1)$$

$$\phi_2 = \left| \frac{1}{2}, \frac{1}{2} \right\rangle \otimes \left| \frac{T}{2}, \frac{1}{2} \right\rangle \otimes \left| \frac{1}{2}, -\frac{1}{2} \right\rangle, \quad (A2)$$

$$\phi_3 = \left| \frac{1}{2}, -\frac{1}{2} \right\rangle \otimes \left| \frac{T}{2}, \frac{1}{2} \right\rangle \otimes \left| \frac{1}{2}, \frac{1}{2} \right\rangle, \quad (A3)$$

$$\phi_4 = \left| \frac{1}{2}, -\frac{1}{2} \right\rangle \otimes \left| \frac{T}{2}, \frac{3}{2} \right\rangle \otimes \left| \frac{1}{2}, -\frac{1}{2} \right\rangle, \quad (A4)$$
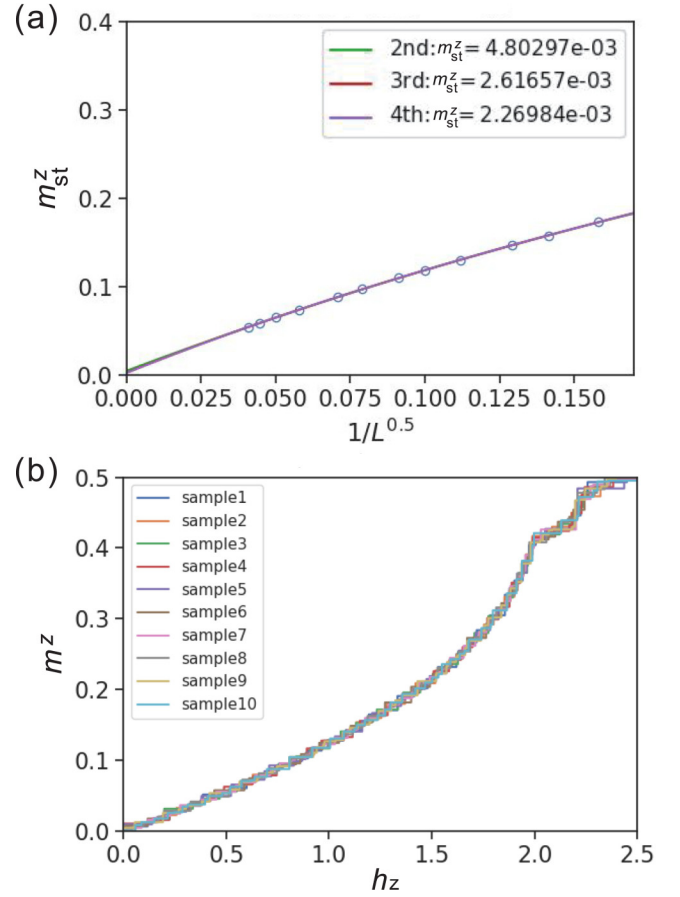

FIG. 16. (a) Finite-size scaling analysis of the staggered magnetization m_{st}^z calculated by DMRG. The parameters are $\Delta_{imp} = 1.1$ and $n_{imp} = 0.1$. Each point is obtained by averaging over $10\,000/L$ samples of random impurity distribution. (b) DMRG results for the uniform magnetization m^z as a function of external field. The magnetization curves for 10 random samplings of impurity distribution with $L = 1000$ are shown.

where $|jm\rangle$ are the simultaneous eigenstates of the angular momentum quantum number j and the angular momentum projection onto the z axis m. For the case of $\Delta_{imp} = 1$, this problem can be easily solved. The ground-state energy is $\varepsilon_0 = -(T + 2)/2$ and the eigenfunction is

$$\psi_{g.s.}(\Delta_{imp} = 1) = A\left(\phi_1 - \phi_2 - \phi_3 + \sqrt{\frac{T + 3}{T - 1}} \phi_4 \right) \quad (A5)$$

with $A = \sqrt{\frac{T-1}{4T}}$. If T is small enough, the dominant configuration of ground state may be written as

$$\psi_{g.s.}(\Delta_{imp} = 1) \approx \left| \frac{1}{2}, -\frac{1}{2} \right\rangle \otimes \left| \frac{T}{2}, \frac{3}{2} \right\rangle \otimes \left| \frac{1}{2}, -\frac{1}{2} \right\rangle. \quad (A6)$$

This means that S^z is maximum at the impurity site. Thus, we conclude that the $S = \frac{1}{2}$ states are localized around the $S_{imp} > 1$ impurity. Since the approximation (A6) approaches the exact ground state with increasing Δ_{imp}, the localization of $S = \frac{1}{2}$ states is stronger for larger Δ_{imp}.
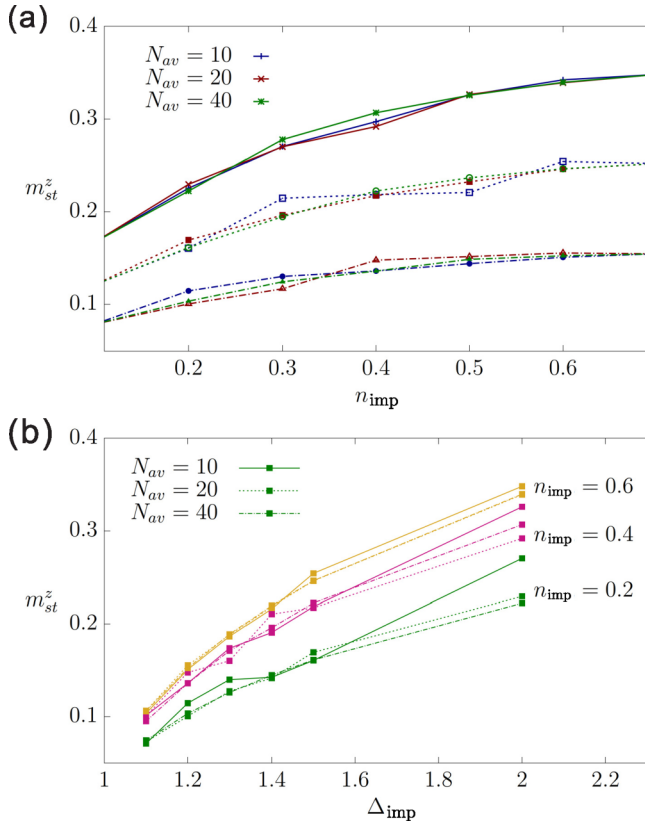
FIG. 17. (a) Variations of m_{st}^z with n_{imp} for averaging over different number of random configurations for $\Delta_{imp} = 1.2$ (dotted-dashed lines), $\Delta_{imp} = 1.5$ (dashed lines), $\Delta_{imp} = 2.0$ (solid lines). (b) Variation of m_{st}^z with Δ_{imp} with increasing N_{av} for $n_{imp} = 0.2$, 0.4, and 0.6.
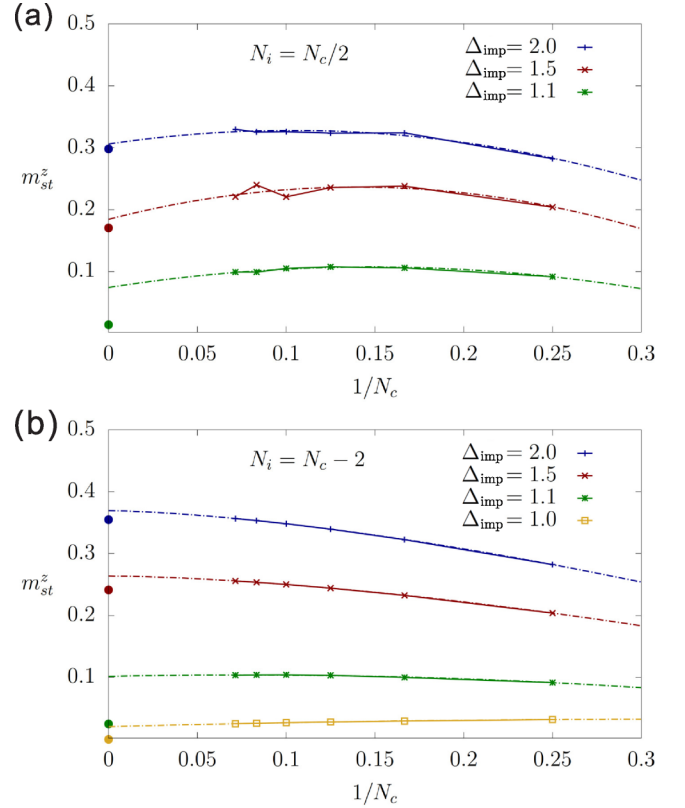

FIG. 18. Cluster-size scaling of m_{st}^z for various Δ_{imp} with the number of impurities (a) $N_i = N_c/2$ and (b) $N_i = N_c - 2$. Average is taken for the maximum of 10 random configurations. Dotted-dashed lines are power-law fits. Solid circles are the results computed using DMRG for corresponding Δ_{imp} and n_{imp}.

In the limit of $\Delta_{imp} = 0$, the ground state is

$$\psi_{\text{g.s.}}(\Delta_{imp} = 0)$$

$$= B \left(\frac{T+1}{\sqrt{T^2 + 2T - 1}} \phi_1 - 2\phi_2 - 2\phi_3 + \sqrt{\frac{T^2 + 2T - 3}{T^2 + 2T - 1}} \phi_4 \right)$$

$$(A7)$$

with $B = 1/\sqrt{10}$. The bases (A2) and (A3) have larger coefficients. Thus, we find that the localization of $S = \frac{1}{2}$ states is released for smaller Δ_{imp}.

APPENDIX B: FINITE-SIZE SCALING AND RANDOM SAMPLING IN DMRG CALCULATIONS

Figure 16(a) shows a finite-scaling analysis of the staggered magnetization m_{st}^z at $\Delta_{imp} = 1.1$ and $n_{imp} = 0.1$, which is one of the most difficult cases to perform the scaling analysis because of small extrapolated value in the thermodynamic limit $L \to \infty$. Fittings with the third- and fourth-order polynomial functions of $l = \sqrt{L}$ lead to $m_{st}^z = 2.617 \times 10^{-3}$ and $m_{st}^z = 2.270 \times 10^{-3}$ in the limit $L \to \infty$, respectively. They are sufficiently close to each other and the fitting lines seem to be reasonable as shown in Fig. 16(a). Thus, we can confirm the validity of the finite-scaling analysis of m_{st}^z.

Figure 16(b) shows the uniform magnetization m^z as a function of external field at $\Delta_{imp} = 1.1$ and $n_{imp} = 0.1$. The magnetization curves for 10 random samplings of impurity distribution with $L = 1000$ are plotted. Since we see only small deviations among the magnetization curves with different random sampling, a system with $L = 1000$ may be large enough to reproduce every phenomenon induced by impurity doping. To gain further accuracy, we average m^z over 10 random samplings to the magnetization curve shown in the main text.

APPENDIX C: SAMPLING OF RANDOM CONFIGURATIONS IN CMFT CALCULATIONS

Staggered magnetization is averaged over various random distributions of impure bonds for a fixed number of impurities. Figure 17 shows the dependence of m_{st}^z with increasing number of random configurations considered for averaging. Due to small cluster sizes, the number of configurations for $n_{imp} = 0.1$ and 0.8 cannot be increased. It is evident from Fig. 17(a) that the fluctuations appearing in m_{st}^z can be minimized by increasing the number of configurations. Figure 17(b) depicts the dependence of the number of configurations for different Δ_{imp}. It suggests that the dependence of m_{st}^z on N_{av} is more significant for lower $n_{imp} = 0.2$ and 0.4.

APPENDIX D: FINITE-SIZE EFFECTS IN CMFT CALCULATIONS

Figure 18 shows m_{st}^z for the number of impurities (N_i) fixed to $N_c/2$ and $N_c - 2$ for respective cluster sizes. Fluctuations for the case of $N_i = N_c/2$ appear as the average is taken for very small number of random configurations ($N_{av} = 10$). We observe that m_{st}^z increases with increasing cluster size up to a certain cluster size, after which it starts to decrease. Power-law fits to the data suggest that on further increasing the size, m_{st}^z will reach the value closer to the one obtained by DMRG [solid circles in Fig. 18(a)]. For $N_i = N_c - 2$, finite-size scaling analysis shows an increase in m_{st}^z with increasing N_c. This is counterintuitive as for completely isotropic Ising ($\Delta \to \infty$) or Heisenberg ($\Delta = 1$) spin chain, where m_{st}^z decreases with system size. However, in our approach, the MF bond remains Heisenberg type while the impure bonds are XXZ type or, in the extreme case, Ising type. For $N_c = 4$, the number of impure bonds within the cluster is 3, while there are two mean-field decoupled Heisenberg bonds. With increasing number of spins in a cluster, the ratio of impure bonds to pure bonds keeps on increasing as the number of isotropic MF bonds remains the same. Due to this competition among Heisenberg bonds and Ising-type (XXZ-type) bonds, m_{st}^z increases with system size, and eventually saturates towards its maximum possible value. Solid circles in Fig. 18(b) show the results obtained by DMRG corresponding to $n_{imp} = 0.8$. Power-law fits of CMFT cluster-size scaling show that the agreement with DMRG results is higher for larger anisotropy in comparison to $\Delta_{imp} = 1.1$.

[1] J. S. Dugdale, *The Electrical Properties of Disordered Metals* (Cambridge University Press, Cambridge, 2005).

[2] A. Maeda, T. Yabe, S. Takebayashi, M. Hase, and K. Uchinokura, Substitution of 3d metals for Cu in $Bi_2(Sr_{0.6}Ca_{0.4})_3Cu_2O_y$, Phys. Rev. B **41**, 4112 (1990).

[3] P. W. Anderson, Absence of diffusion in certain random lattices, Phys. Rev. **109**, 1492 (1958).

[4] T. Ying, Y. Gu, X. Chen, X. Wang, S. Jin, L. Zhao, W. Zhang, and X. Chen, Anderson localization of electrons in single crystals: LixFe7Se8, Sci. Adv. **2**, 2 (2016).

[5] Y. Imry and M. Wortis, Influence of quenched impurities on first-order phase transitions, Phys. Rev. B **19**, 3580 (1979).

[6] F. Hammerath, S. Nishimoto, H.-J. Grafe, A. U. B. Wolter, V. Kataev, P. Ribeiro, C. Hess, S.-L. Drechsler, and B. Büchner, Spin Gap in the Zigzag Spin-1/2 Chain Cuprate $Sr_{0.9}Ca_{0.1}CuO_2$, Phys. Rev. Lett. **107**, 017203 (2011).

[7] S. Eggert and I. Affleck, Magnetic impurities in half-integer-spin Heisenberg antiferromagnetic chains, Phys. Rev. B **46**, 10866 (1992).

[8] F. Anfuso and S. Eggert, Interaction effects between impurities in low-dimensional spin-(1/2) antiferromagnets, Europhys. Lett. **73**, 271 (2006).

[9] M. Hagiwara, K. Katsumata, I. Affleck, B. I. Halperin, and J. P. Renard, Observation of S = 1/2 Degrees of Freedom in an S = 1 Linear-Chain Heisenberg Antiferromagnet, Phys. Rev. Lett. **65**, 3181 (1990).

[10] M. Hase, I. Terasaki, Y. Sasago, K. Uchinokura, and H. Obara, Effects of Substitution of Zn for Cu in the Spin-Peierls Cuprate, $CuGeO_3$: The Suppression of the Spin-Peierls Transition and the Occurrence of a New Spin-Glass State, Phys. Rev. Lett. **71**, 4059 (1993).

[11] B. Grenier, L. Regnault, J. Lorenzo, J. Bossy, J. Renard, G. Dhalenne, and A. Revcolevschi, Effect of magnetic field and Si-doping on the spin-Peierls phase of $CuGeO_3$, Phys. B (Amsterdam) **234-236**, 534 (1997).

[12] M. Azuma, Y. Fujishiro, M. Takano, M. Nohara, and H. Takagi, Switching of the gapped singlet spin-liquid state to an antiferromagnetically ordered state in $Sr(Cu_{1-x}Zn_x)_2O_3$, Phys. Rev. B **55**, R8658(R) (1997).

[13] N. Motoyama, H. Eisaki, and S. Uchida, Magnetic Susceptibility of Ideal Spin 1/2 Heisenberg Antiferromagnetic Chain Systems, Sr_2CuO_3 and $SrCuO_2$, Phys. Rev. Lett. **76**, 3212 (1996).

[14] K. M. Kojima, J. Yamanobe, H. Eisaki, S. Uchida, Y. Fudamoto, I. M. Gat, M. I. Larkin, A. Savici, Y. J. Uemura, P. P. Kyriakou, M. T. Rovers, and G. M. Luke, Site-dilution in the quasi-one-dimensional antiferromagnet $Sr_2(Cu_{1-x}Pd_x)O_3$: Reduction of néel temperature and spatial distribution of ordered moment sizes, Phys. Rev. B **70**, 094402 (2004).

[15] G. Simutis, S. Gvasaliya, M. Månsson, A. L. Chernyshev, A. Mohan, S. Singh, C. Hess, A. T. Savici, A. I. Kolesnikov, A. Piovano, T. Perring, I. Zaliznyak, B. Büchner, and A. Zheludev, Spin Pseudogap in Ni-Doped $SrCuO_2$, Phys. Rev. Lett. **111**, 067204 (2013).

[16] K. Karmakar, R. Bag, M. Skoulatos, C. Rüegg, and S. Singh, Impurities in the weakly coupled quantum spin chains Sr_2CuO_3 and $SrCuO_2$, Phys. Rev. B **95**, 235154 (2017).

[17] S. Kimura, M. Matsuda, T. Masuda, S. Hondo, K. Kaneko, N. Metoki, M. Hagiwara, T. Takeuchi, K. Okunishi, Z. He, K. Kindo, T. Taniyama, and M. Itoh, Longitudinal Spin Density Wave Order in a Quasi-1D Ising-Like Quantum Antiferromagnet, Phys. Rev. Lett. **101**, 207201 (2008).

[18] A. K. Bera, B. Lake, W.-D. Stein, and S. Zander, Magnetic correlations of the quasi-one-dimensional half-integer spin-chain antiferromagnets $SrM_2V_2O_8(M = Co, Mn)$, Phys. Rev. B **89**, 094402 (2014).

[19] Y. Utz, F. Hammerath, R. Kraus, T. Ritschel, J. Geck, L. Hozoi, J. van den Brink, A. Mohan, C. Hess, K. Karmakar, S. Singh, D. Bounoua, R. Saint-Martin, L. Pinsard-Gaudart, A. Revcolevschi, B. Büchner, and H.-J. Grafe, Effect of different in-chain impurities on the magnetic properties of the spin chain compound $SrCuO_2$ probed by NMR, Phys. Rev. B **96**, 115135 (2017).

[20] S. Eggert, D. P. Gustafsson, and S. Rommer, Phase Diagram of an Impurity in the Spin-1/2 Chain: Two-Channel Kondo Effect Versus Curie Law, Phys. Rev. Lett. **86**, 516 (2001).

[21] J. Bobroff, N. Laflorencie, L. K. Alexander, A. V. Mahajan, B. Koteswararao, and P. Mendels, Impurity-Induced Magnetic Order in Low-Dimensional Spin-Gapped Materials, Phys. Rev. Lett. **103**, 047201 (2009).

[22] L. K. Alexander, J. Bobroff, A. V. Mahajan, B. Koteswararao, N. Laflorencie, and F. Alet, Impurity effects in coupled-ladder

BiCu$_2$PO$_6$ studied by NMR and quantum Monte Carlo simulations, Phys. Rev. B **81**, 054438 (2010).

[23] W. Zhang, J.-I. Igarashi, and P. Fulde, Thermodynamics of an impurity coupled to a Heisenberg chain: Density-matrix renormalization group and Monte Carlo studies, J. Phys. Soc. Jpn. **66**, 1912 (1997).

[24] W. Zhang, J. Igarashi, and P. Fulde, Magnetic impurity coupled to a Heisenberg chain: Density-matrix renormalization-group study, Phys. Rev. B **56**, 654 (1997).

[25] S. R. White, Density Matrix Formulation for Quantum Renormalization Groups, Phys. Rev. Lett. **69**, 2863 (1992).

[26] S. Eggert and I. Affleck, Impurities in $S = 1/2$ Heisenberg Antiferromagnetic Chains: Consequences for Neutron Scattering and Knight Shift, Phys. Rev. Lett. **75**, 934 (1995).

[27] M. Laukamp, G. B. Martins, C. Gazza, A. L. Malvezzi, E. Dagotto, P. M. Hansen, A. C. López, and J. Riera, Enhancement of antiferromagnetic correlations induced by nonmagnetic impurities: Origin and predictions for NMR experiments, Phys. Rev. B **57**, 10755 (1998).

[28] H. Frahm and A. A. Zvyagin, The open spin chain with impurity: An exact solution, J. Phys.: Condens. Matter **9**, 9939 (1997).

[29] I. Affleck, D. Gepner, H. J. Schulz, and T. Ziman, Critical behaviour of spin-S Heisenberg antiferromagnetic chains: Analytic and numerical results, J. Phys. A: Math. Gen. **22**, 511 (1989).

[30] R. R. P. Singh, M. E. Fisher, and R. Shankar, Spin-1/2 antiferromagnetic XXZ chain: New results and insights, Phys. Rev. B **39**, 2562 (1989).

[31] L. Hulthén, Arkiv Math. Astron. Fys., **26a**, 11 (1938).

[32] C. N. Yang and C. P. Yang, One-dimensional chain of anisotropic spin-spin interactions. I. Proof of Bethe's hypothesis for ground state in a finite system, Phys. Rev. **150**, 321 (1966).

[33] C. N. Yang and C. P. Yang, One-dimensional chain of anisotropic spin-spin interactions. II. Properties of the ground-state energy per lattice site for an infinite system, Phys. Rev. **150**, 327 (1966).

[34] A. Luther and I. Peschel, Calculation of critical exponents in two dimensions from quantum field theory in one dimension, Phys. Rev. B **12**, 3908 (1975).

[35] N. Bogoliubov, A. Izergin, and V. Korepin, Critical exponents for integrable models, Nucl. Phys. B **275**, 687 (1986).

[36] M. Takigawa, N. Motoyama, H. Eisaki, and S. Uchida, Field-induced staggered magnetization near impurities in the S = 1/2 one-dimensional Heisenberg antiferromagnet Sr$_2$CuO$_3$, Phys. Rev. B **55**, 14129 (1997).

[37] S. R. White, I. Affleck, and D. J. Scalapino, Friedel oscillations and charge density waves in chains and ladders, Phys. Rev. B **65**, 165122 (2002).

[38] S. Wessel and S. Haas, Three-dimensional ordering in weakly coupled antiferromagnetic ladders and chains, Phys. Rev. B **62**, 316 (2000).

[39] J. Des Cloizeaux and M. Gaudin, Anisotropic linear magnetic chain, J. Math. Phys. **7**, 1384 (1966).

[40] S. Kimura, T. Takeuchi, K. Okunishi, M. Hagiwara, Z. He, K. Kindo, T. Taniyama, and M. Itoh, Novel Ordering of an S = 1/2 Quasi-1d Ising-Like Antiferromagnet in Magnetic Field, Phys. Rev. Lett. **100**, 057202 (2008).

[41] D. C. Johnston, R. K. Kremer, M. Troyer, X. Wang, A. Klumper, S. L. Bud'ko, A. F. Panchula, and P. C. Canfield, Thermodynamics of spin S = 1/2 antiferromagnetic uniform and alternating-exchange Heisenberg chains, Phys. Rev. B **61**, 9558 (2000).

[42] W. Liu, B. Zhu, L. Zhang, Y. Ke, and C. Lee, Edge states in quantum spin chains: The interplay among interaction, gradient magnetic field, and floquet engineering, Phys. Rev. A **104**, 023305 (2021).